Modular reconfiguration of hybrid PV-TEG systems via artificial rabbit algorithm: Modelling, design and HIL validation

Bo Yang [a], Yulin Li [a], Jianxiang Huang [b], Miwei Li [a], Ruyi Zheng [a], Jinhang Duan [a], Tingsheng Fan [a], He Zou [a], Tao Liu [c], Jingbo Wang [d,*], Hongchun Shu [a], Lin Jiang [d]

[a] *Faculty of Electric Power Engineering, Kunming University of Science and Technology, 650500 Kunming, China*
[b] *Kunming Bureau of CSG EHV Transmission Company, 650217 Kunming, China*
[c] *Faculty of Science, Kunming University of Science and Technology, 650500 Kunming, China*
[d] *Department of Electrical Engineering and Electronics, University of Liverpool, L69 3GJ Liverpool, UK*

HIGHLIGHTS

- A hybrid PV-TEG system model is introduced and constructed in this work;
- A modular reconfiguration scheme for hybrid PV-TEG systems is proposed, in which the PV and TEG array components are modularized to reduce the overall costs;
- This work devises a reconfiguration method for hybrid systems based on ARO algorithm;
- The HIL experiment based on RTLAB platform is undertaken to further prove the implementation feasibility of the reconfiguration strategy.

ARTICLE INFO

Keywords:
Hybrid PV-TEG systems
Modular reconfiguration
Artificial rabbit optimization
Hardware-in-the-loop

ABSTRACT

To further improve the power generation efficiency of traditional photovoltaic (PV) systems, this paper designs a theoretical model of a hybrid power generation system that consists of the individual PV system and thermoelectric generation (TEG) system. Meanwhile, partial shielding condition (PSC) is a common but serious problem during operation that might lead to power loss and component mismatch in hybrid PV-TEG system. Therefore, a reconfiguration method for the hybrid PV-TEG system based on artificial rabbit optimization (ARO) algorithm is proposed in this study to alleviate the negative impact caused by PSC and thus improve the power generation efficiency of the hybrid system. ARO algorithm is applied to adjust the switching matrix of the hybrid system to change the electrical connection among PV arrays and TEG arrays, and thus further to reduce the adverse effect of PSC and maximize the output power of the hybrid system. To verify the effectiveness of the proposed method, simulation tests are carried out on 4 × 4 and 20 × 15 arrays, respectively. For a quantitative and fair comparison, this work employs maximum output power, average output power, mismatch loss, and standard deviation as evaluation indexes, upon which four different algorithms including GA, PSO, WOA, AOA and ACO are thoroughly compared. Simulation results show that the output power of the hybrid system after ARO algorithm based reconfiguration is improved by 34.05% in the 4 × 4 array and 23.10% in the 20 × 15 array, respectively. In addition, hardware-in-the-loop (HIL) experiments are carried out based on RTLAB platform to verify the hardware feasibility of the proposed reconfiguration strategy.

1. Introduction

As the global power demand and the price of traditional energy sources (coal, natural gas) are rising, the process of promoting the transformation of global energy structure and the development of renewable energy is accelerating. For instance, according to the "14th Five-Year Plan for Modern Energy System" proposed by China, the large-scale and high-quality development of wind and photovoltaic (PV) will be strongly promoted [1–3]. Meanwhile, according to the latest UK Energy Security Strategy, the installed PV capacity in the UK is expected to increase fivefold by 2035. In addition, the European Union amended its Act on renewable energy development to specify the target of increasing the share of renewable energy in the energy mix to 45% by

* Corresponding author.
E-mail address: JingboWang96@outlook.com (J. Wang).

Nomenclature

Variable

V_{out}	total output voltage
I_{out}	total output current
V_{maxi}	output voltage in row i
I_{ij}	output current in row i and column j
P_{pv}	total output power
V_i	voltage of the ith row
c	mapping vector
I_i	current of the ith row
V_{oc}	open circuit voltage
R_i	internal resistance
T_h	temperature of the hot side
T_c	temperature of the cold side
T_{avg}	average temperature on both sides of TEG
ΔT	temperature difference between the two sides of TEG
R_L	load
I_s	total output current
R_{s_in}	total internal resistance
V_{s_oc}	equivalent voltage
T_p	surface temperature
T_e	ambient temperature
G	solar radiation
ν_f	ambient wind speed
$\overrightarrow{V}_i(t+1)$	candidate position of the ith rabbit at the time $t+1$
$\overrightarrow{P}_i$	position of the ith rabbit,
R	running factor
L	movement pace during the detour foraging action
H	hiding parameter
P_{miss}	Mismatch loss
P_{Mum}	maximum output power without partial occlusion
P_M	maximum output power under PSC
P_{re}	Power increase percentage
P_{Mre}	maximum output power after reconfiguration
P_{Mbe}	maximum output power before reconfiguration
$Npop$	population size
k_{max_iter}	the maximum iterations number

Abbreviations

AOA	Arithmetic optimization algorithm
ARO	Artificial rabbit optimization
BL	Bridge linked
GA	Genetic algorithm
HIL	Hardware-in-the-loop
HC	Honey comb
LMPPs	local MPPs
MPPT	maximum power point tracking
NTD	non-uniform temperature distribution
PSC	Partial shielding condition
PSO	Particle swarm optimization
PV	Photovoltaic
SP	Series-parallel
STD	Standard deviation
TCT	Total cross tied
TEG	Thermoelectric generation
WOA	Whale optimization algorithm

Parameter

M	number of rows
N	number of and columns
β_1	-2.579
β_2	0.014
μ_0	the basic part of Seebeck coefficient
μ_1	the rate of change of Seebeck coefficient
n	the size of population

2030. Overall, the PV industry will still play an important role in future energy structure transformation and development [4,5].

Recently, solar power generation, as an important component of renewable energy systems, has received widespread attention from researchers on how to improve the utilization rate of solar energy. [6,7]. During PV power generation, it is difficult for PV modules to fully utilize the solar insolation, most of the radiation is dissipated into the environment in the form of heat, resulting in PV module temperature rise. However, this temperature rise of PV modules will adversely affect the PV power generation efficiency [8,9]. Therefore, an appropriate solution is needed to effectively collect and re-utilize this extra solar thermal energy for further power generation. One feasible way is to combine the PV system with the thermoelectric generation (TEG) system as hybrid PV-TEG system for higher power generation efficiency, in which the TEG system can generate electricity from the waste heat dissipated by PV modules to maximize the use of solar energy to generate electricity [10–12]. Reference [13] proposes a coupling system that consists of PV modules, TEG modules, and thermoelectric cooler, in which the effects of irradiance and temperature on system operation performance are also analyzed. Reference [14] presents a comprehensive multi-objective optimization method for a concentrated spectrum splitting PV-TEG hybrid system.

Due to the limitations that result from its inherent power generation mechanism, the power generation efficiency of PV system is relatively low and easily influenced by the external operation environments. First, the partial shielding condition (PSC) of sunlight leads to the unbalanced power generation efficiency of PV modules, which reduces the output power of the PV system. By placing TEG modules below PV modules, the common PSCs in PV systems not only result in non-uniform irradiance distribution on PV arrays but also leads to uneven heat distribution on TEG modules. In detail, TEG arrays receive waste heat from PV arrays and longer-wavelength infrared waves from solar radiation, and then experience a non-uniform temperature distribution (NTD). Second, the PSC will cause the temperature rise of shielded PV modules, resulting in the hotspot effect that will reduce the power generation efficiency and even cause damage to the PV modules. To alleviate the negative impacts of PSC on PV power generation, bypass diodes are connected in parallel to isolate the shielded modules, but this measurement will lead to the appearance of multiple local MPPs (LMPPs) on output power-voltage (*P-V*) curve. Similarly, multiple LMPPs also tend to appear on the TEG power-time (*P-T*) characteristic due to the NTD. Therefore, in theory, the *P-T* curve of PV-TEG hybrid systems may exhibit more complex multiple peaks. To solve this, many maximum power point tracking (MPPT) technologies are applied under PSC to extract the maximum power point [15–17]. Reference [18] uses artificial bee colony algorithm and simultaneous heat transfer search algorithm to improve the MPPT accuracy and speed. An MPPT controller based on model predictive control is proposed in reference [19] to track the maximum power point under rapid irradiance change. Apart from the aforementioned MPPT strategies, reconfiguration technology has also been applied to solve this problem in recent years and achieved desirable results.

The purpose of the reconfiguration technology is to properly allocate the topologies of PV arrays under the PSC to obtain the maximum output power [20]. In general, reconfiguration technologies are mainly divided into static and dynamic reconfiguration. Static reconfiguration strategically changes the physical position of the PV modules so that the

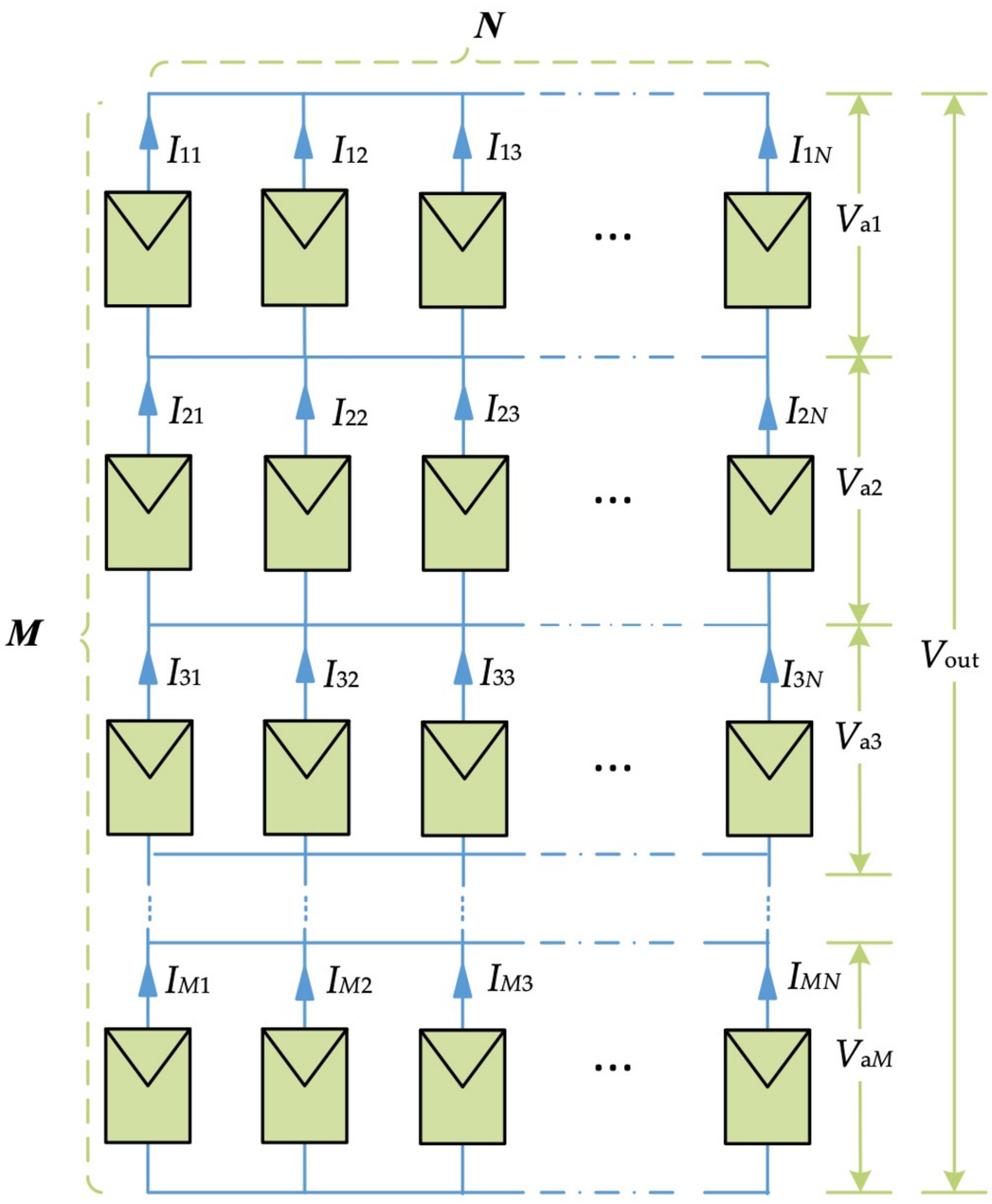

Fig. 1. $M \times N$ TCT connected structure of the PV array.

shadow can be evenly distributed on all the arrays. Although the static reconfiguration technology is relatively simple in principle, it is difficult to cope with complex PSC problems for large-scale PV arrays. In contrast, dynamic reconfiguration dynamically changes the electrical interconnection among different modules based on a switching matrix, which is more suitable for the reconfiguration problem under different PSCs [21]. In reference [22], a PV reconfiguration method is proposed based on the butterfly optimization algorithm to extract the maximum power point. In reference [23], based on the new peak power estimation theory, genetic algorithm is applied to the reconfiguration of total cross tied (TCT) PV arrays. Reference [24] proposes a socio-inspired democratic political algorithm based PV reconfiguration strategy to improve the power generation efficiency of PV systems.

However, reconfiguration methods are barely investigated and applied in PV-TEG systems for maximum energy harvesting though they have been proven as effective and reliable solutions. Therefore, the aim of this study is to develop and evaluate an optimal reconfiguration scheme based on the artificial rabbit optimization (ARO) algorithm for hybrid PV-TEG systems to mitigate the negative impacts of PSC on power generation efficiency, and the main contributions are outlined as follows:

- For the first time, a modular hybrid PV-TEG system reconfiguration model has been established, aiming to reduce a series of adverse effects brought about by PSC to enhance output power. Based on this, the solar energy utilization rate can be maximized while effectively reducing the number of switching actions, which further saves operation costs and prolongs the equipment service life;
- To the best knowledge of the authors, the reconfiguration problem of a hybrid PV-TEG system has been proposed and studied for the first time. In this study, a reconfiguration scheme for PV-TEG hybrid systems is developed and validated, which aims to mitigate the negative impacts of PSC on power generation efficiency of the proposed PV-TEG hybrid system;
- An ARO algorithm based optimal reconfiguration scheme is developed for the hybrid system, in which the ARO algorithm can effectively balance the global exploration and local exploitation via the energy factor mechanism. Therefore, the global searching ability of this algorithm is largely improved, upon which the optimal reconfiguration schemes can be quickly and reliably obtained;
- For a comprehensive and in-depth evaluation of the proposed reconfiguration method, two different PV-TEG array sizes of 4×4 and 20×15 are adopted for simulation tests and analysis. Meanwhile, multiple different types of PSCs are considered to further verify the generality of the reconfiguration method;
- Finally, a hardware-in-the-loop (HIL) experiment is carried out to testify to the implementation feasibility of the proposed reconfiguration strategy.

The rest of the paper is arranged as follows: Section 2 introduces the modelling of the PV system, TEG system, and hybrid PV-TEG system. Section 3 presents the ARO algorithm based reconfiguration method for the hybrid system. The simulation tests and results are illustrated in Section 4. The results of HIL experiments based on the RTLAB platform are showed and analyzed in Section 5. Section 6 outlines the main contribution of this work and future perspectives.

2. Hybrid PV-TEG system modelling

2.1. PV system modelling

PV arrays adopt the $M \times N$ TCT connected structure, as shown in Fig. 1. Compared with the bridge linked (BL), series-parallel (SP) structure, and honey comb (HC) structure, TCT structure can effectively improve the operation stability and efficiency of PV arrays under the PSC [25–28]. The total output voltage V_{out} and current I_{out} are presented by

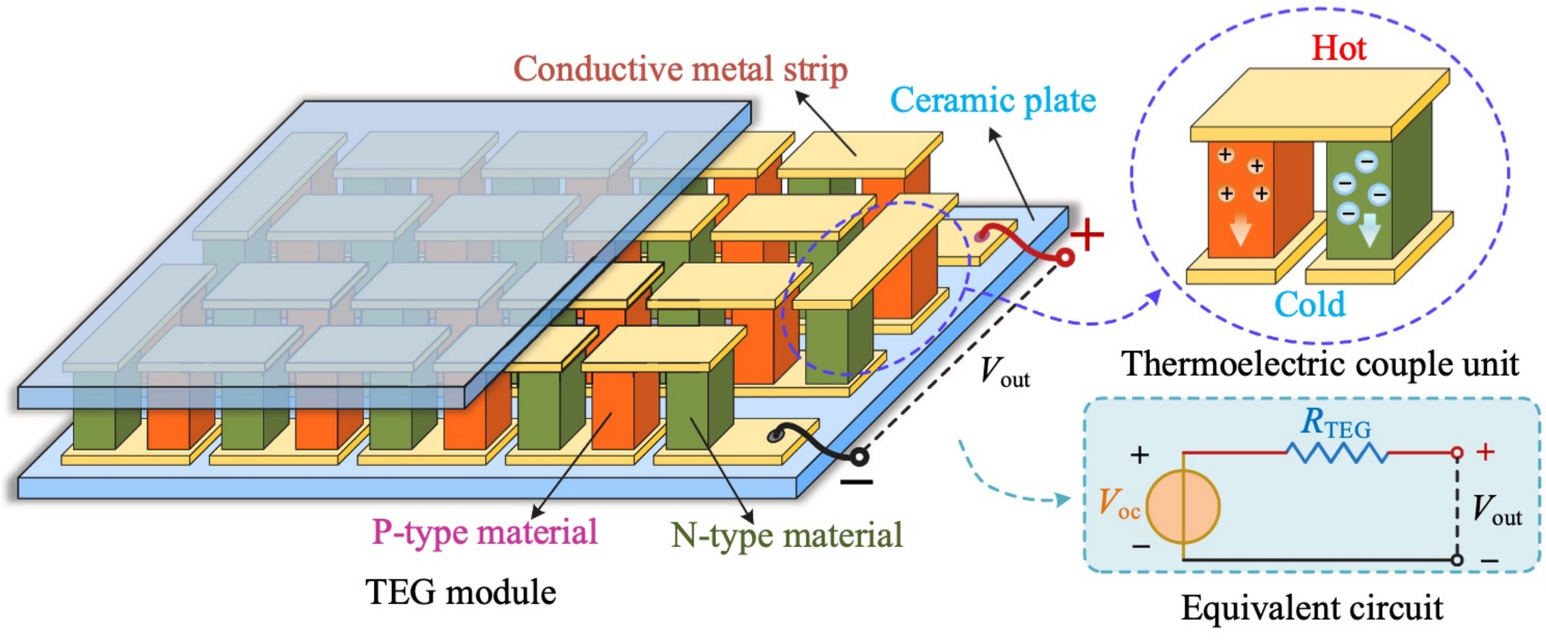

Fig. 2. Schematic diagram of the TEG system.

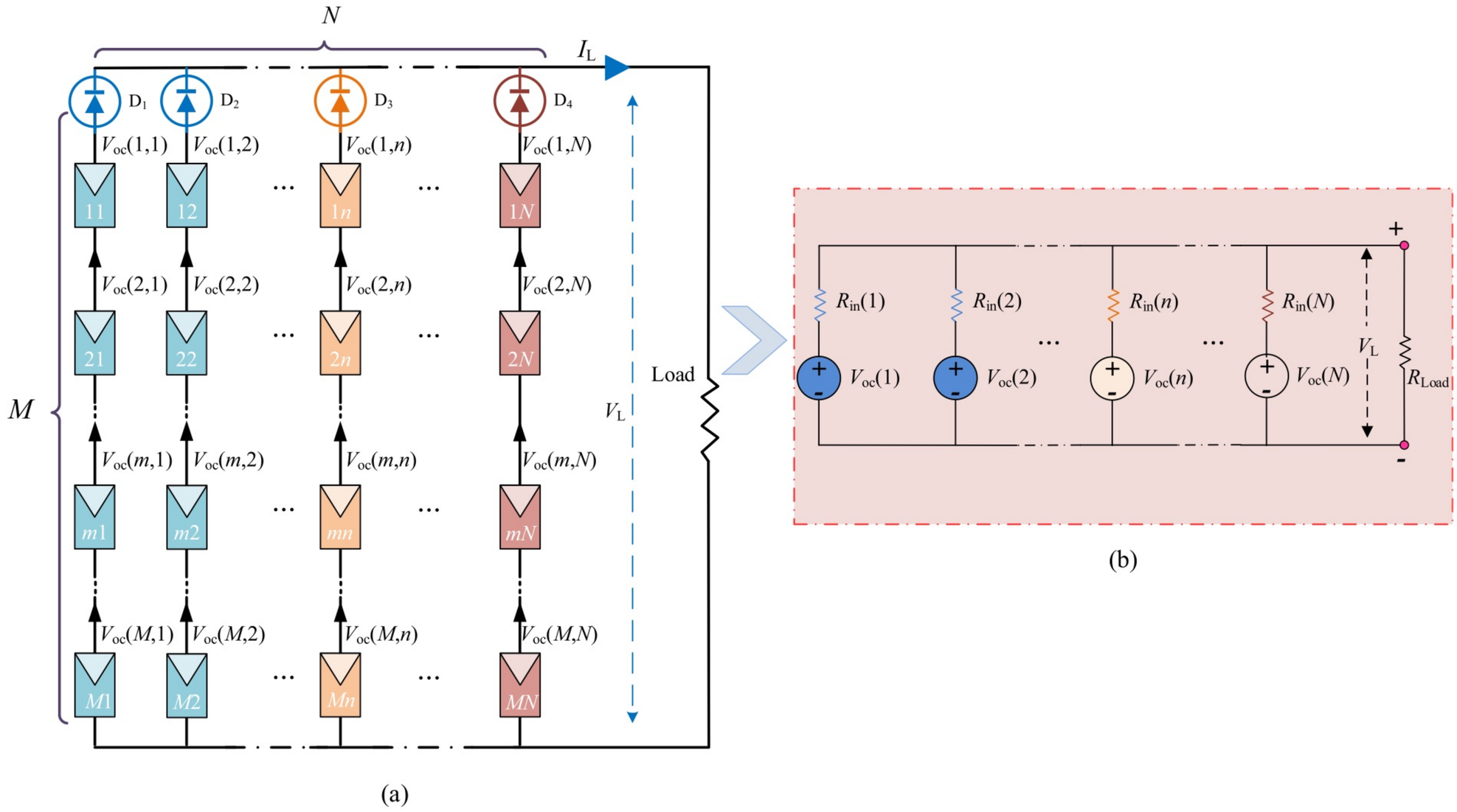

Fig. 3. Model of the TEG array.

$$V_{\text{out}} = \sum_{i=1}^{M} V_{maxi} \tag{1}$$

$$I_{\text{out}} = \sum_{i=1}^{M} \left(I_{ij} - I_{(i+1)j}\right) = 0, j = 1, 2, \ldots, N \tag{2}$$

where M and N are the number of rows and columns, respectively. V_{maxi} is the output voltage in row i. I_{ij} is the output current in row i and column j. Therefore, the total output power P_{pv} of the PV array is

$$P_{\text{pv}} = \sum_{i=1}^{M} V_i * I_i \tag{3}$$

where V_i and I_i are the current and voltage of the ith row, respectively.

2.2. TEG system modelling

TEG is a device that is convert heat into electricity, as shown in Fig. 2 [29–31]. The open circuit voltage V_{oc} and internal resistance R_{i} of the TEG module can be calculated according to the temperature at both ends, as follows:

$$V_{\text{oc}} = \mu \Delta T = \mu (T_{\text{h}} - T_{\text{c}}) \tag{4}$$

$$R_{\text{in}} = \beta_1 + \beta_2 \cdot T_{\text{avg}} = \beta_1 + \beta_2 \cdot \frac{(T_{\text{h}} - T_{\text{c}})}{2} \tag{5}$$

where T_{h} and T_{c} are the temperature of the hot side and cold side, respectively. T_{avg} is the average temperature on both sides. ΔT is the temperature difference. $\beta_1 = -2.579$, $\beta_2 = 0.014$. μ is Seebeck's coefficient, which can be calculated by

$$\mu\left(T_{\text{avg}}\right) = \mu_0 + \mu_1 ln\left(T_{\text{avg}}/T_{\text{ref}}\right) \tag{6}$$

where $\mu_0 = 210\ \mu\text{V/K}$ and $\mu_1 = 120\ \mu\text{V/K}$ are the basic part and rate of change of Seebeck coefficient, respectively. T_{ref} is the reference temperature. Therefore, when TEG module is connected with load R_{L}, its working current is expressed as

$$I = \frac{V_{\text{oc}}}{R_{\text{L}} + R_{\text{in}}} \tag{7}$$

The output power is described by

$$P_L = \left(\frac{V_{\text{oc}}}{R_{\text{L}} + R_{\text{in}}}\right)^2 R_{\text{L}} \tag{8}$$

In this work, the $M \times N$ TEG array is adopted, as shown in Fig. 3(a). Therefore, according to Eqs. (4) and (5), the equivalent voltage source $V_{\text{oc}}(n)$ and equivalent resistance $R_{\text{in}}(n)$ of each column can be obtained as follows:

$$V_{\text{oc}}(n) = \sum_{m=1}^{M} V_{\text{oc}}(m, n), n = 1, \ldots, N \tag{9}$$

$$R_{\text{in}}(n) = \sum_{m=1}^{M} R_{\text{in}}(m, n), n = 1, \ldots, N \tag{10}$$

where V_{oc} and R_{in} are the open circuit voltage and internal resistance, respectively. V_{oc} and R_{in} are the total open-circuit voltage and total internal resistance, respectively. Therefore, the entire array can be equivalent to N voltage sources in parallel, as shown in Fig. 3(b).

Each column of the TEG array can be equivalent to current source connected, and the current source is represented by

$$I(n) = \frac{V_{\text{oc}}(n)}{R_{\text{in}}(n)}, n = 1, \ldots, N \tag{11}$$

where $I(n)$ is the output current in column n, The total output current I_s and total internal resistance $R_{\text{s\_in}}$ of the entire TEG array are presented as

$$I_s = \sum_{n=1}^{N} I(n) \tag{12}$$

$$R_{\text{s\_in}} = \frac{1}{\sum_{n=1}^{N} \frac{1}{R_{\text{in}}(n)}} \tag{13}$$

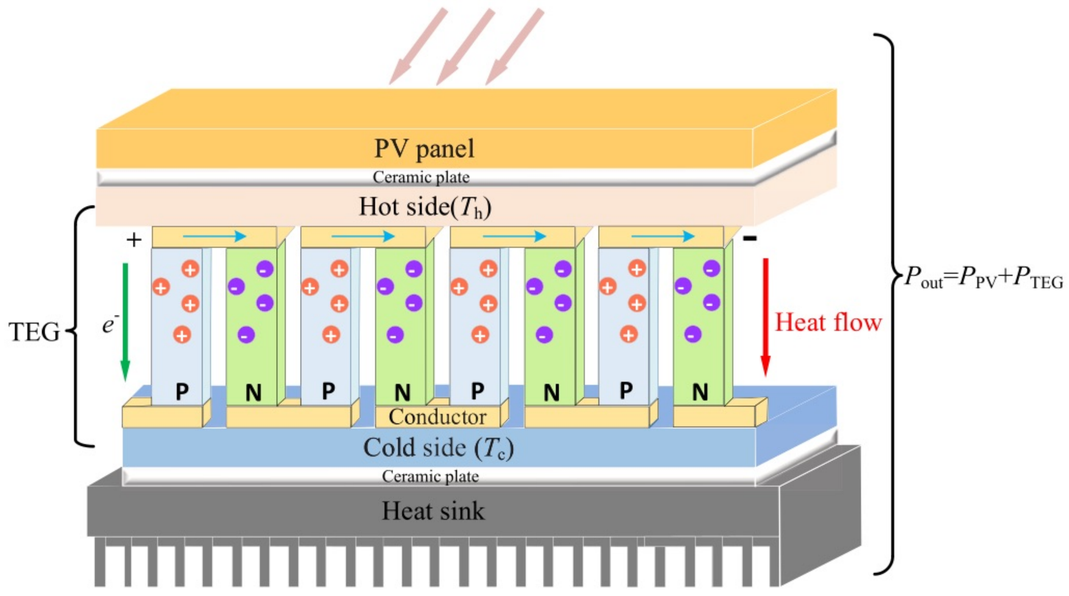

Fig. 4. Hybrid PV-TEG structure schematic diagram.

Table 1
Modular results of various PV sizes.

Array size	#1	#2	#3	#4	#5
4 × 4	4 × 2	4 × 2	–	–	–
20 × 15	15 × 3	15 × 3	15 × 3	15 × 3	15 × 3

Table 2
Modular results of various TEG sizes.

Array size	#1	#2	#3	#4	#5
4 × 4	2 × 4	2 × 4	–	–	–
20 × 15	4 × 15	4 × 15	4 × 15	4 × 15	4 × 15

Then, the current source is converted into a voltage source by using Thevenin's theorem, and its equivalent voltage V_{s_oc} is shown in Eq. (14). The maximum output power of the TEG array is calculated by

$$V_{s\_oc} = R_{s\_in} \cdot I_s \tag{14}$$

$$P_{s\_max} = \frac{V_L^2}{R_{load}} = \frac{\left(\frac{1}{2}V_{s\_oc}\right)^2}{R_{s\_in}} = \frac{V_{s\_oc}^2}{4R_{s\_in}} \tag{15}$$

2.3. Hybrid PV-TEG system modelling

The hybrid PV-TEG system is shown in Fig. 4. The surface temperature T_p is calculated by [32,33].

$$T_p = 0.943T_e + 0.0195G - 0.528\nu_f + 0.3529 \tag{18}$$

where T_e is the ambient temperature, G is the solar radiation, and ν_f is the ambient wind speed.

Therefore, the total output power is

$$P_{out} = P_{PV} + P_{TEG} \tag{19}$$

where P_{out} is the output power of PV-TEG hybrid system. P_{PV} and P_{TEG} are the output power of PV system and TEG system, respectively.

In addition, considering that the use of switching devices will lead to the increase of reconfiguration cost and increase the complexity of PV-TEG arrays reconfiguration. Therefore, this work adopts modular array reconfiguration method, i.e., the array is divided into several appropriate blocks according to the array size for reconfiguration, so as to reduce the number of switches and computational complexity. The modular results of PV-TEG arrays studied in this work are shown in Table 1 and Table 2.

3. Reconfiguration of PV-TEG hybrid system based on ARO algorithm

ARO algorithm is a new developed swarm intelligent optimization algorithm proposed by Prof. Wang in 2022, which is inspired by the survival strategies of rabbits in nature [34,35]. The main algorithm model and optimization principle are introduced in this section.

3.1. Optimization principle of ARO

3.1.1. Detour foraging

The detour foraging strategy means that rabbits in the wild usually avoid their own nests and choose to travel further to forage, which can be expressed as:

$$\begin{aligned}\vec{V}_i(t+1) &= \vec{P}_i(t) + R\cdot\left(\vec{P}_i(t) - \vec{P}_j(t)\right) + \text{round}(0.5\cdot(0.05+a_1))\cdot n_1, i, j \\ &= 1,\ldots,n \text{ and } j \neq i\end{aligned} \tag{20}$$

where $\vec{V}_i(t+1)$ represents the candidate position, $\vec{P}_i(t)$ and $\vec{P}_j(t)$ represent the position of rabbit at time t, respectively. a_1 is the random number in (0,1), and R is represented as the running factor of the rabbit's running characteristics that can be obtained by

$$R = L\cdot c \tag{21}$$

$$L = \left(e - e^{\left(\frac{t-1}{T}\right)^2}\right)\cdot sin(2\pi a_2) \tag{22}$$

$$c = \begin{cases} 1, \text{if } k == g(l) \\ 0, \text{else} \end{cases}, k = 1,\ldots,d \text{ and } l = 1,\ldots,\lceil a_3\cdot d\rceil \tag{23}$$

$$g = \text{randperm}(d) \tag{24}$$

$$n_1 \sim N(0,1) \tag{25}$$

where L represents the movement pace during the detour foraging action. The relatively large value of L is conducive to exploration, while its relatively small value of L is beneficial for exploitation. a_2 and a_3 denote random numbers in (0,1), T represents the number of iterations, n represents the size of population, d represents the dimension, c is a mapping vector. $\lceil\cdot\rceil$ is the ceiling function. The detour foraging behavior will strengthen the global searching capability.

3.1.2. Random hiding

The random hiding means that in each iteration, each rabbit will generate d burrows along each dimension and randomly select one of all burrows to hide. The jth burrow of the ith rabbit is described by

$$\vec{b}_{i,j}(t) = \vec{x}_i(t) + H\cdot g\cdot\vec{x}_i(t), i = 1,\ldots,n \text{ and } j = 1,\ldots,d \tag{26}$$

$$H = \frac{T-t+1}{T}\cdot a_4 \tag{27}$$

$$n_2 \sim N(0,1) \tag{28}$$

$$g(k) = \begin{cases} 1, \text{if } k == j \\ 0, \text{else} \end{cases}, k = 1,\ldots,d \tag{29}$$

where H represents the hiding parameter. To survive, rabbits need to find a burrow to hide in. Therefore, Eqs. (30)–(33) mathematically model this random hiding strategy as

$$\vec{V}_i(t+1) = \vec{x}_i(t) + R\cdot\left(a_4\cdot\vec{b}_{i,r}(t) - \vec{x}_i(t)\right), i = 1,\ldots,n \tag{30}$$

Table 3
The basic optimization framework of ARO.

1. **Input:** Randomly initialize a set of rabbits X_i(solution) and evaluate their fitness Fit_i, and X_{best} is the best solution found so far.
2. **While** the stop criterion is not satisfied do
3. **For** each X_i calculate the energy factor A using Eq. (34).
4. **If** A > 1
5. Choose a rabbit randomly from other individuals.
6. Calculate R by Eqs. (21) ~ (25).
7. Perform detour foraging by (20).
8. Calculate the fitness Fit_i.
9. Update the position of the current individual by Eq. (33).
10. **Else**
11. Generate d burrows and randomly pick one as hiding by Eq. (26).
12. Perform random hiding by Eq. (30).
13. Calculate the fitness Fit_i.
14. Update the position of the current individual by Eq. (33).
15. End If
16. Update the best position found so far X_{best}.
17. **End For**
18. **End While**
19. **Return** X_{best}

$$g_r(k) = \begin{cases} 1, \text{if } k == \lceil a_5 \cdot d \rceil \\ 0, \text{else} \end{cases}, k = 1, \ldots, d \tag{31}$$

$$\vec{b}_{i,r}(t) = \vec{x}_i(t) + H \cdot g_r \cdot \vec{x}_i(t) \tag{32}$$

where $\vec{b}_{i,r}(t)$ is selected cave from d burrows to hide, a_4 and a_5 are two random numbers distributed in (0,1). After performing the detour foraging or random hiding, the position of the ith rabbit is updated as

$$\vec{x}_i(t+1) = \begin{cases} \vec{x}_i(t), f\left(\vec{x}_i(t)\right) \le f\left(\vec{P}_i(t+1)\right) \\ \vec{P}_i(t+1), f\left(\vec{x}_i(t)\right) \rangle f\left(\vec{P}_i(t+1)\right) \end{cases} \tag{33}$$

Therefore, Eq. (33) indicates that when the fitness value of the candidate position is better than the current position, the rabbit will abandon the current position and stay in the generated candidate position.

3.1.3. Energy shrink

ARO algorithm is more inclined to detour foraging in the early iteration, and more inclined to random hiding in the late iteration, which is adjusted by the energy factor that can be described by

$$A(t) = 4\left(1 - \frac{t}{T}\right) ln\frac{1}{a} \tag{34}$$

where a is a random number distributed in (0,1).

When energy factor A>0, rabbits are more likely to take detour foraging as the global exploration phase. Conversely, when the energy factor $A \le 0$, rabbits tend to choose random hiding behaviors as the local exploitation phase. To determine the influence of the energy factor A on ARO algorithm, the probability of A>0 is calculated by

$$P_{\text{probability}} = \{A(t) > 0\} = \frac{\int_0^2 \int_0^{e^{-\frac{1}{2k}}} \mathrm{d}r\mathrm{d}\varepsilon}{1 \cdot 2} = \frac{1}{4} \cdot \int_{-\infty}^{-\frac{1}{4}} \frac{e^t}{t} \mathrm{d}t + e^{-\frac{1}{4}} \approx 0.5 \tag{35}$$

where $\varepsilon = 2 \cdot \left(1 - \frac{t}{T}\right)$. In the ARO algorithm, Eq. (35) shows that the probability of detour foraging and random hiding is almost the same, so the introduction of the energy factor A can result in a good balance during iterations. The optimization mechanism of ARO algorithm is demonstrated in Table 3.

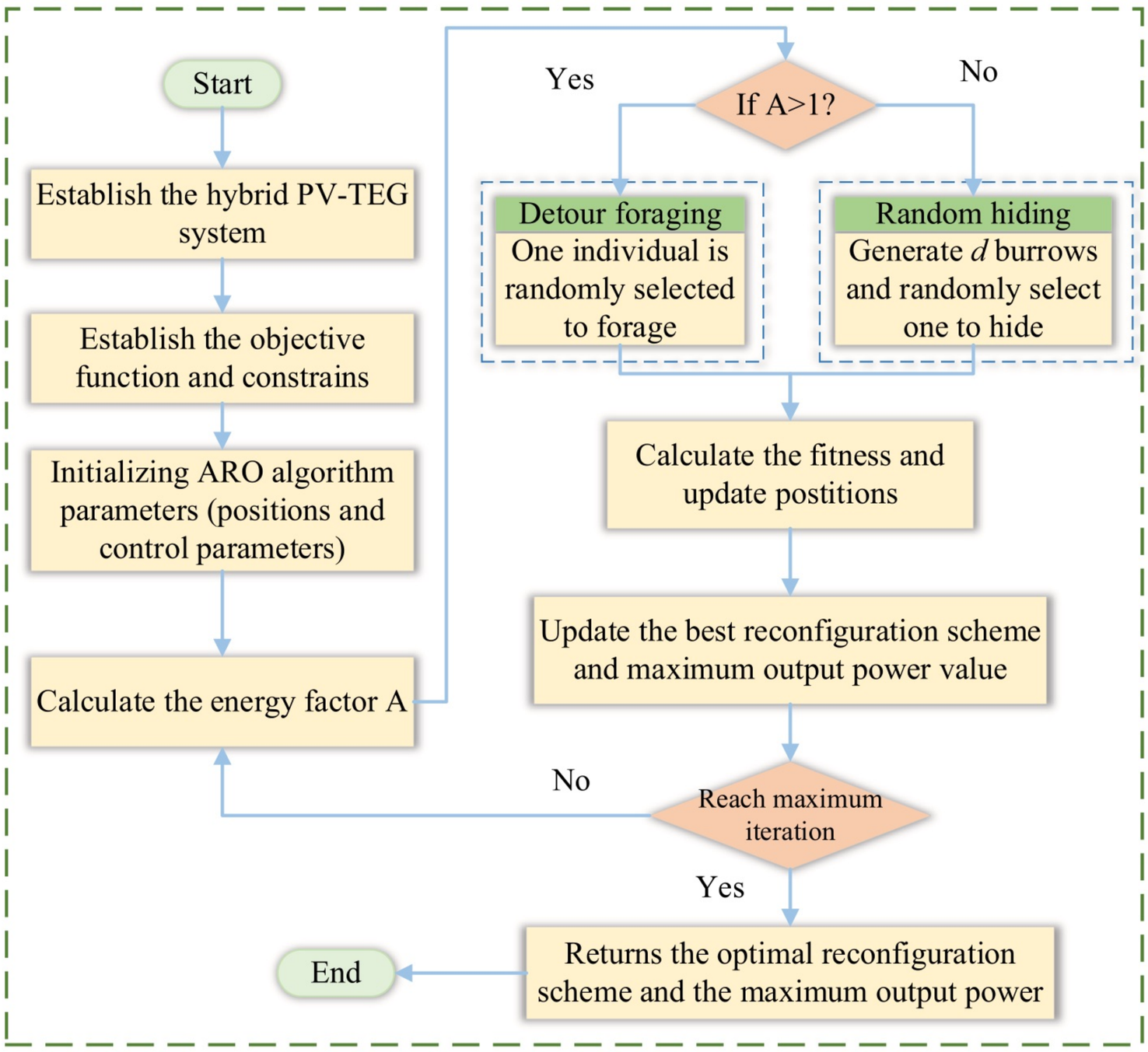

Fig. 5. Implementation procedure of hybrid PV-TEG system reconfiguration based on ARO.

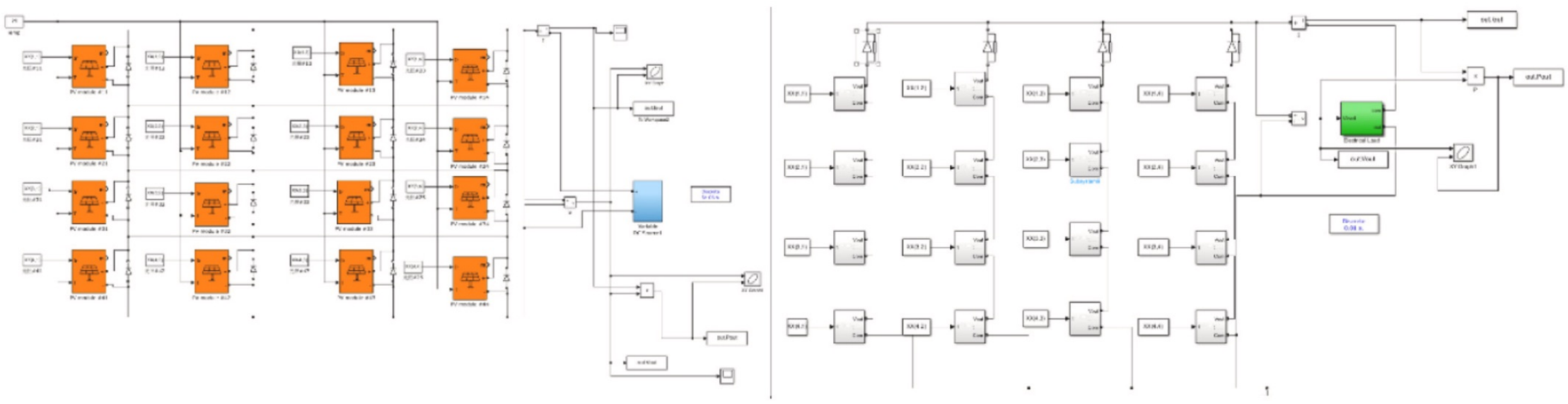

Fig. 6. Simulink model of the 4 × 4 array.

Table 4
Parameters of the PV/TEG module.

PV component		TEG component	
Product model	A 10Green Technology AJ-M60–225	**Product model**	TGM199–1.4-2.0
Maximum power (W)	224.9856	**Parameter measurement condition**	$T_c = 30$ °C, $T_h = 200$ °C
The voltage of the maximum power(V)	30.24	**Size of module**	40 mm × 40 mm × 40 mm
The current of the maximum power(A)	7.44	**Maximum output power(W)**	7.3
Open-circuit voltage(V)	36.24	**Open-circuit voltage(V)**	11
Open-circuit current(A)	8.04	**Open-circuit current(A)**	2.65
Number of batteries per component	60	**Number of thermoelectric units**	$n_{np} = 199$

3.2. Design for reconfiguration of hybrid PV-TEG system based on ARO algorithm

3.2.1. Objective function and constraints

Reconfiguration of hybrid PV-TEG systems is designed to increase the potential maximum output power. Therefore, the total power output of the overall system is selected as the indicator of the objective function F, as follows:

$$F = max(P_{PV} + P_{TEG}) \tag{36}$$

Each component in the PV system only exchanges with another component in the same column, changing the row number. Therefore, the state quantity of an electrical switch should meet the following constraints:

$$\begin{cases} x_{i,j} \in \{1, 2, \ldots, M\} \\ \bigcup_{i=1}^{M} x_{i,j} = \{1, 2, \ldots, M\} \end{cases} \tag{37}$$

where $x_{i,j}$ represents the number of the PV component.

Each component in the TEG system only exchanges with another component in the same row, changing the column number. Therefore, the state quantity of an electrical switch should meet the following constraints:

$$\begin{cases} k_{i,j} \in \{1, 2, \ldots, N\} \\ \bigcup_{i=1}^{N} k_{i,j} = \{1, 2, \ldots, N\} \end{cases} \tag{38}$$

where $k_{i,j}$ represents the number of the TEG component.

3.2.2. Reconfiguration of hybrid system

The dynamic reconfiguration of a hybrid system is detailed as follows: Firstly, the sensors collect data such as output current, voltage, and irradiance of the PV array and TEG array. Then, aiming at maximizing the output power, ARO algorithm is used to obtain the optimal irradiation distribution scheme of the arrays according to the obtained optimized parameters. Finally, the switch matrix dynamically changes the electrical connections inside the arrays based on the optimal configuration scheme. The implementation process of hybrid system reconfiguration based on ARO algorithm to control switch matrix actions is shown in Fig. 5.

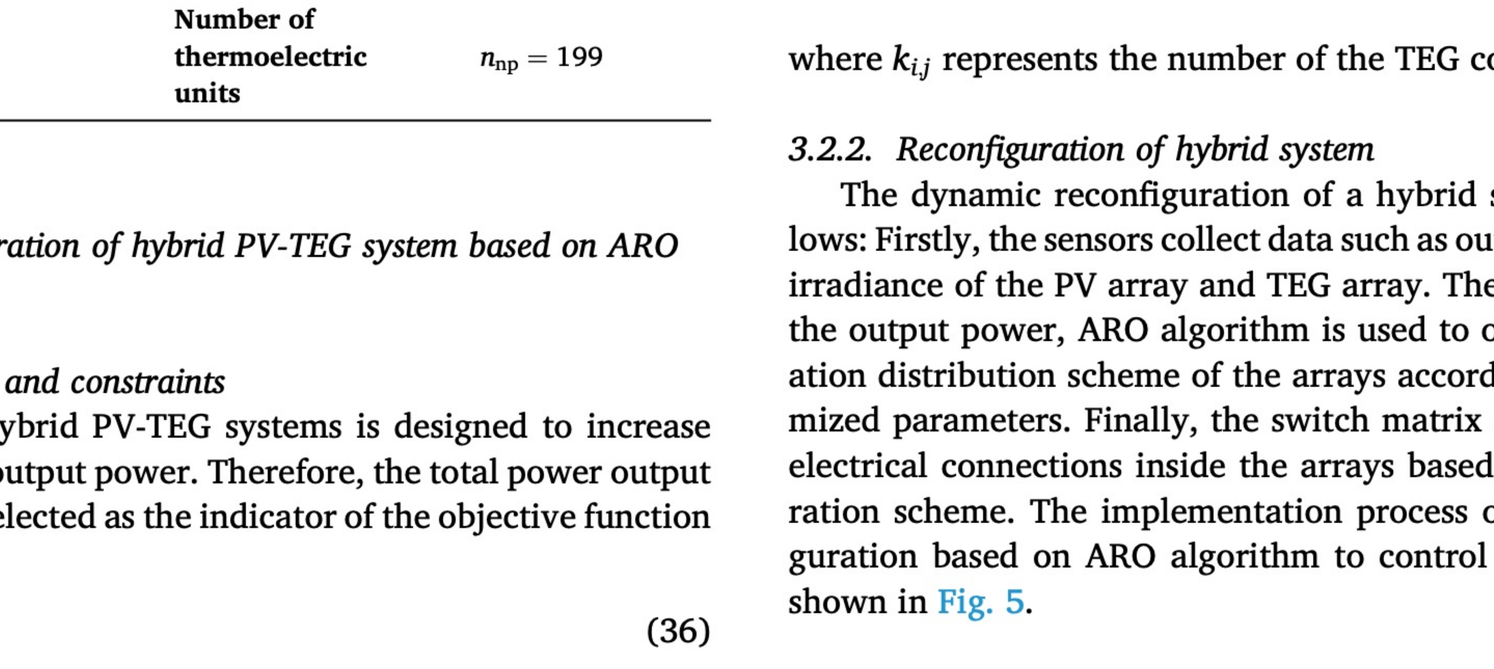

Fig. 7. Actual shading implementation of the 4 × 4 array.

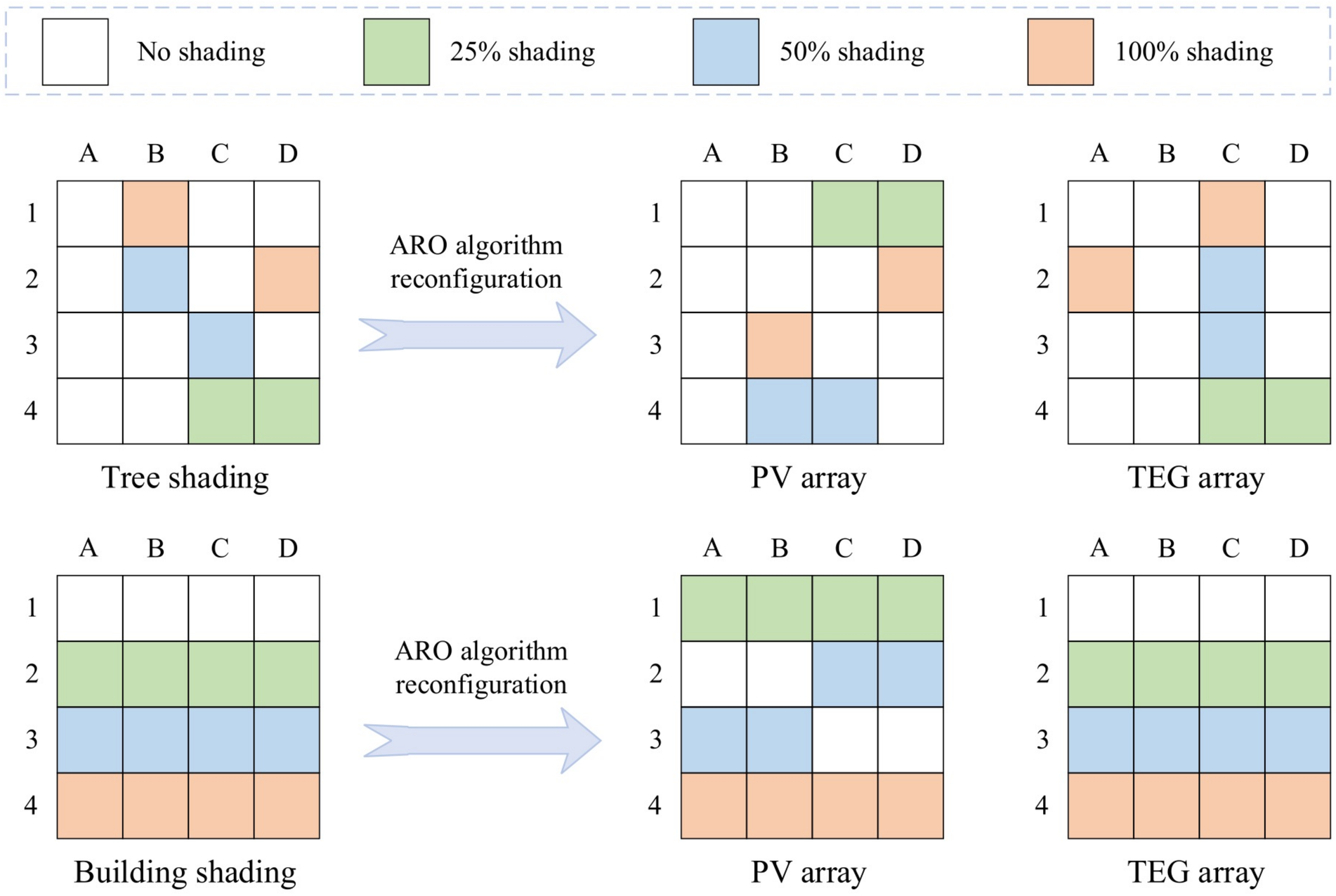

Fig. 8. The irradiance and reconfiguration scheme of the 4 × 4 PV-TEG array [38].

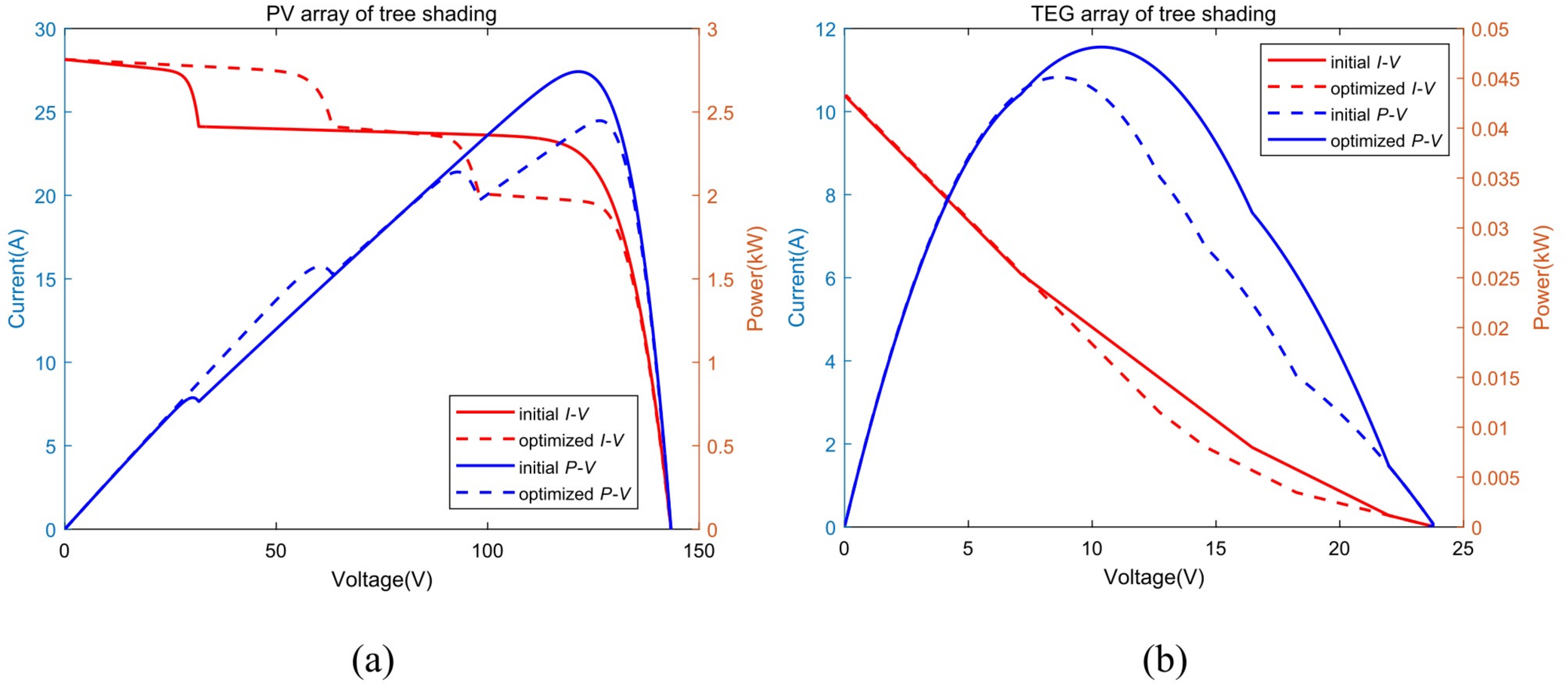

Fig. 9. Output result of the 4 × 4 PV-TEG system before and after reconfiguration under tree shading. (a) Output curve of PV array and (b) Output curve of TEG array.

4. Case studies

4.1. Simulation environment and evaluation indicators

To verify the effectiveness of the proposed reconfiguration method, a series of simulation tests will be firstly conducted on hybrid PV-TEG systems of 4 × 4 and 20 × 15 sizes. Fig. 6 shows the Simulink model of PV array and TEG array at 4 × 4, in which PV array is connected by TCT and TEG array is connected by SP. Meanwhile, for a quantitative analysis of the reconfiguration method, the mismatch loss and power increase percentage are used to evaluate its reconfiguration performance [24]. Mismatch loss P_{miss} refers to the difference between maximum output power P_{Mum} without partial occlusion and maximum output power P_{M} under PSC, as

$$P_{\text{miss}} = P_{\text{Mum}} - P_{\text{M}} \tag{39}$$

Power increase percentage P_{re} refers to the ratio of the difference between the maximum power output before and after reconfiguration to the maximum power output before reconfiguration, as follows:

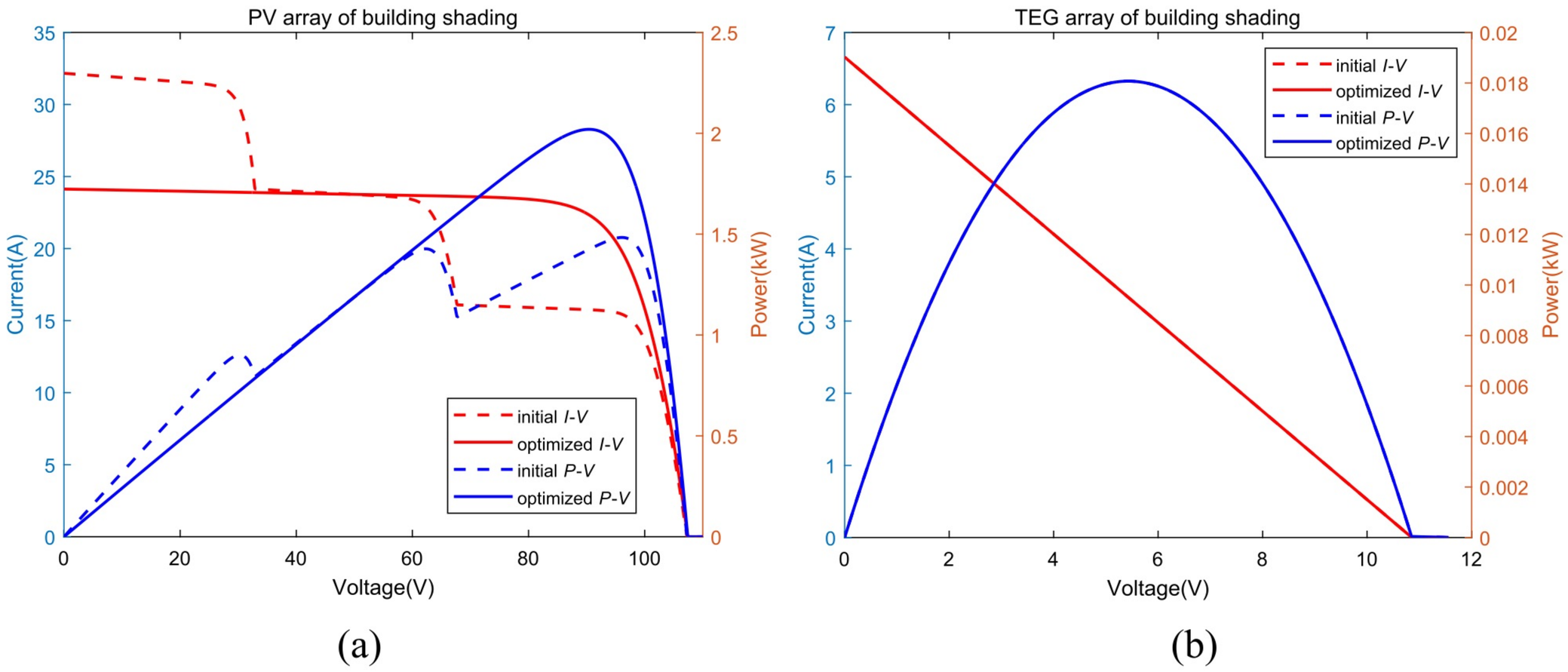

Fig. 10. Output result of 4 × 4 PV-TEG system before and after reconfiguration under building shading. (a) Output curve of PV array and (b) Output curve of TEG array.

Table 5
Results after reconfiguration by ARO algorithm.

Shadow pattern	Before reconfiguration(kW)	ARO	
		P_{max}(kW)	P_{avg}(kW)
Tree shading	2.31	2.76	2.76
Building shading	1.38	2.05	2.05

$$P_{re} = \frac{P_{Mre} - P_{Mbe}}{P_{Mbe}} \times 100\% \tag{40}$$

where P_{Mre} and P_{Mbe} are the maximum output power of the hybrid system before and after reconfiguration, respectively.

In addition, for a comprehensive and fair analysis, particle swarm optimization (PSO) [36,37], genetic algorithm (GA) [37,38], whale optimization algorithm (WOA) [39,40], arithmetic optimization algorithm (AOA) [41], and ant colony algorithm (ACO) are used for

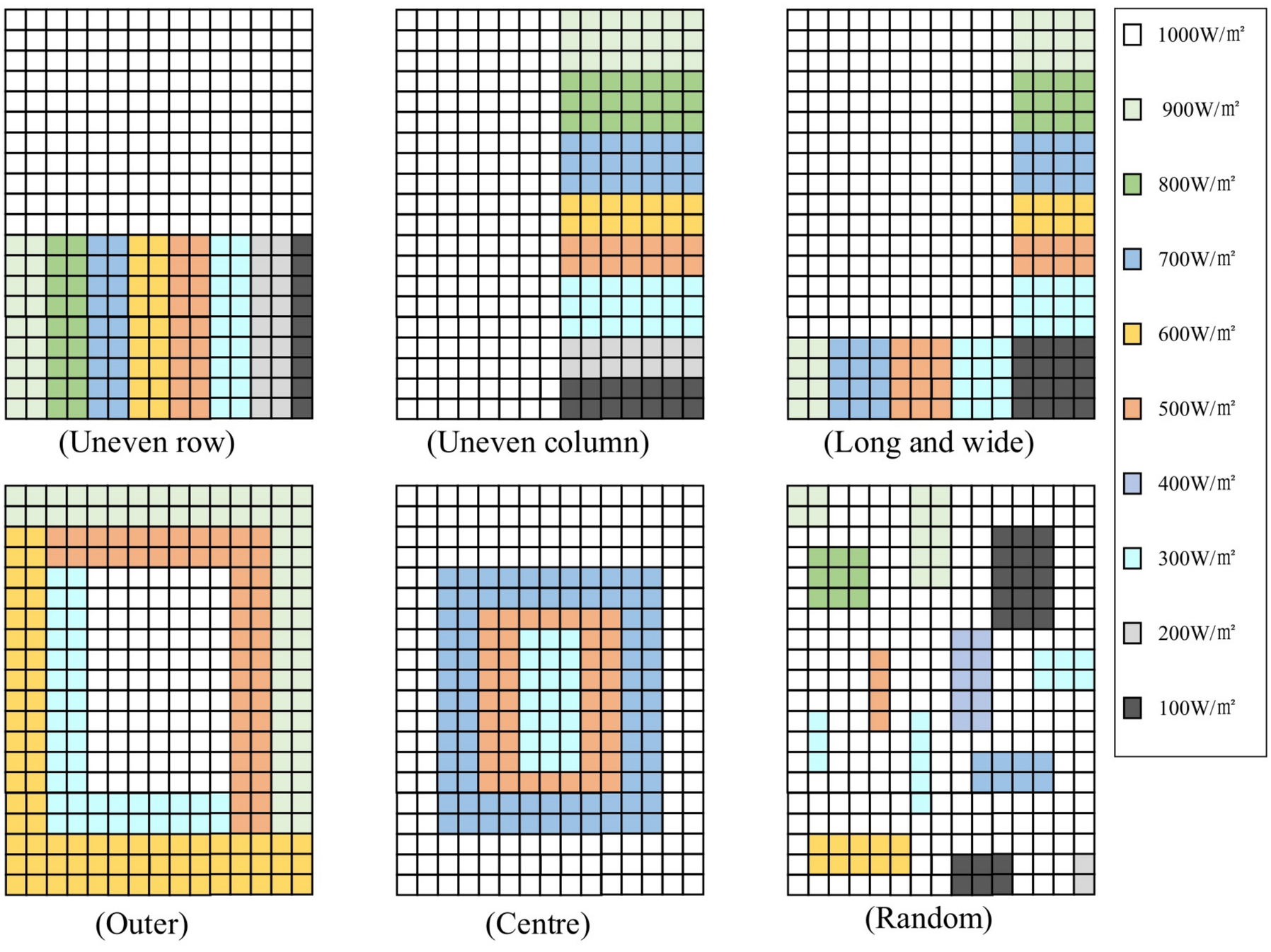

Fig. 11. The irradiance of 20 × 15 PV-TEG array under standard PSC.

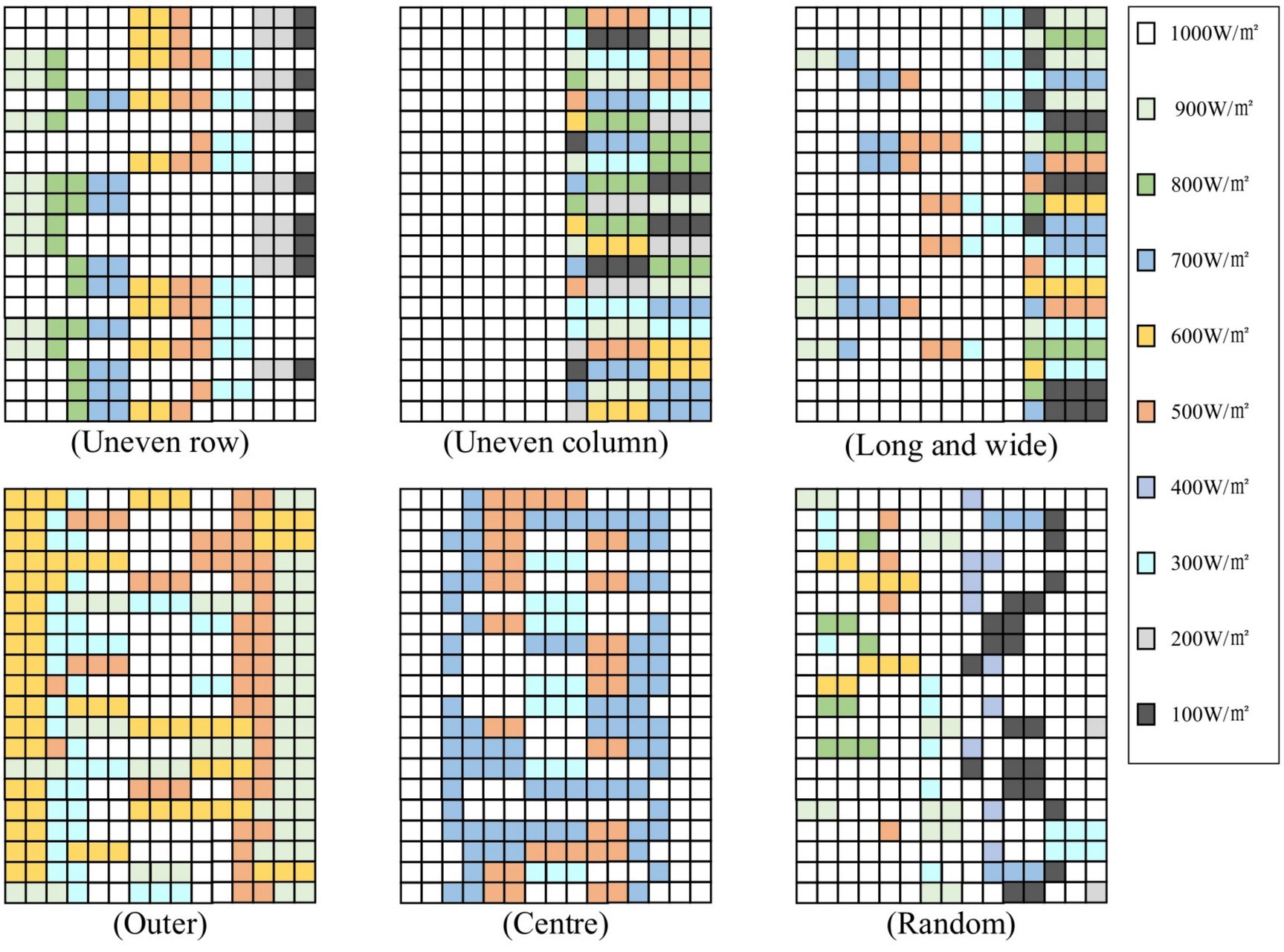

(a) The reconfiguration scheme of PV array

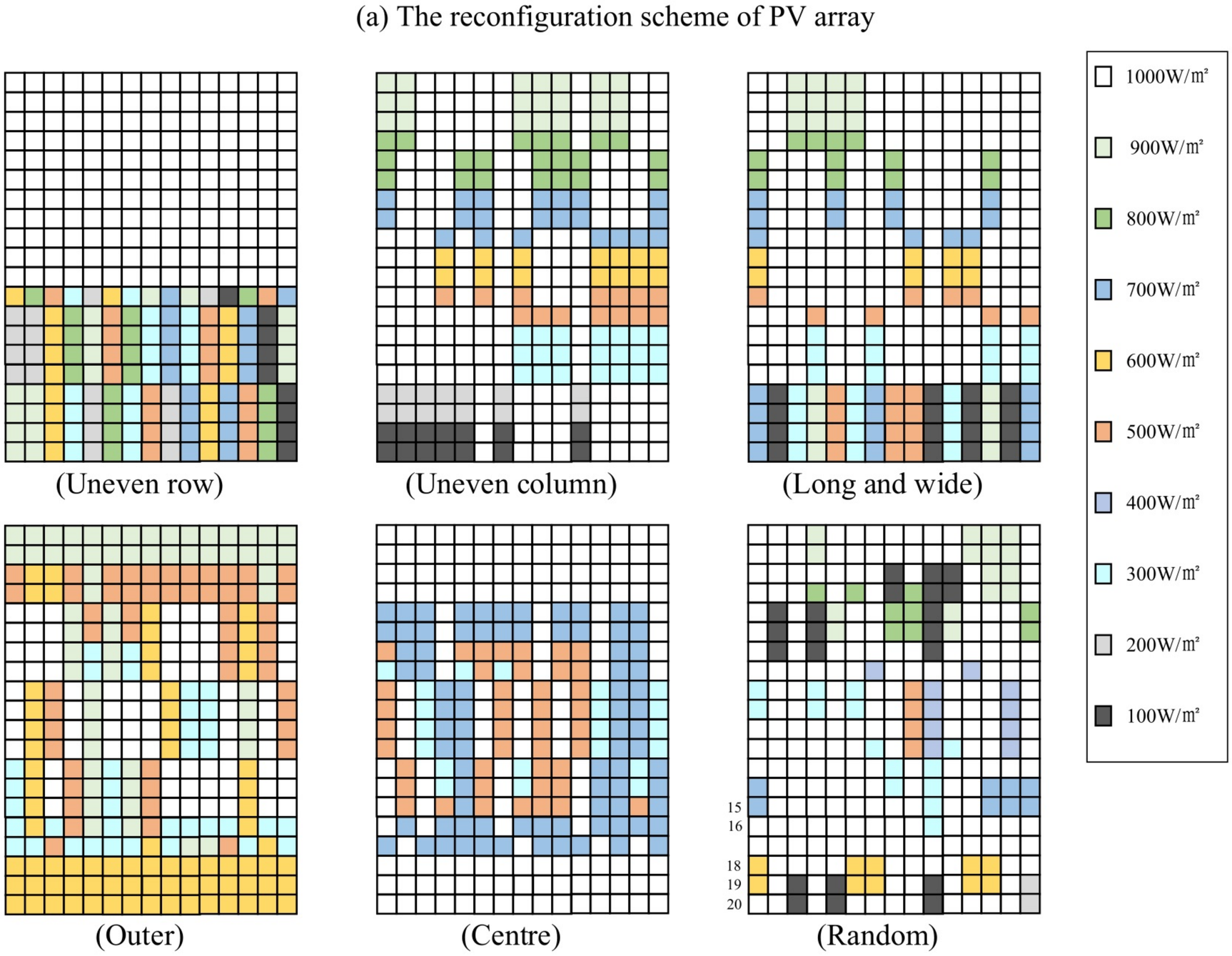

(b) The reconfiguration scheme of TEG array

Fig. 12. The reconfiguration scheme of the 20 × 15 PV-TEG array under standard PSC. (a) The reconfiguration scheme of PV array and (b) The reconfiguration scheme of TEG array.

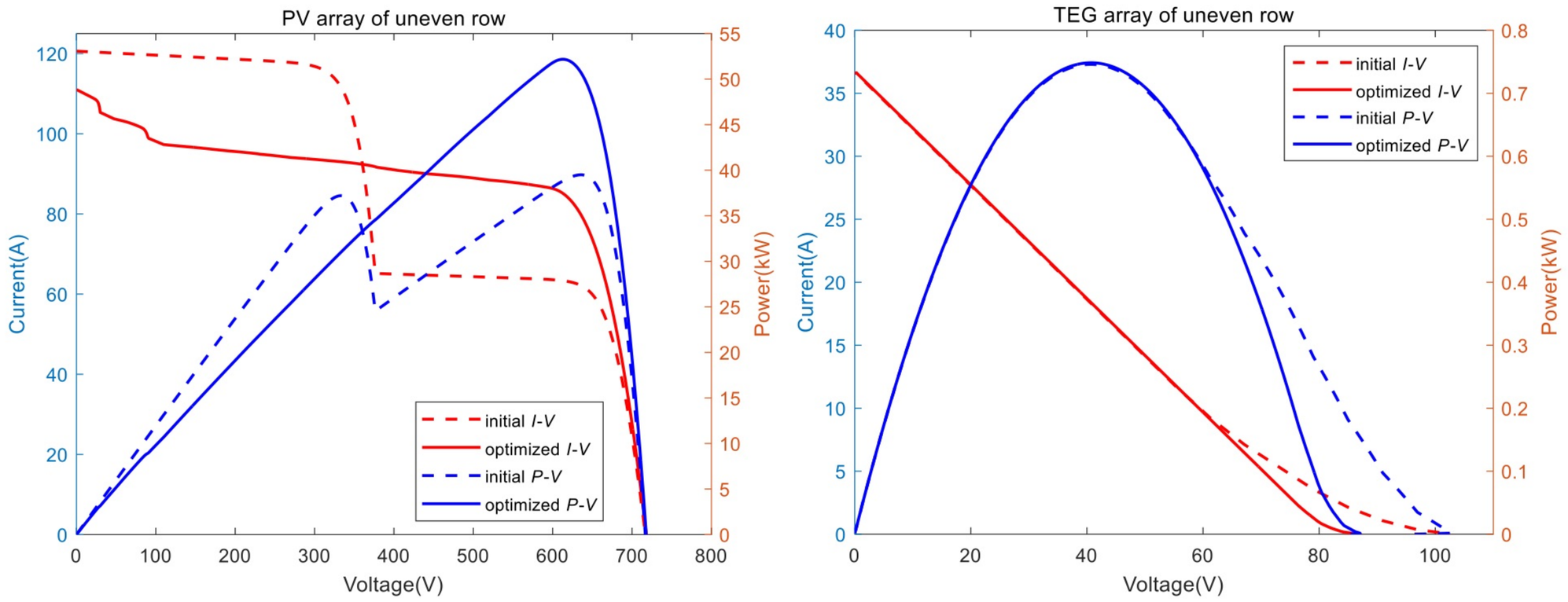

(a) Output curve under uneven row

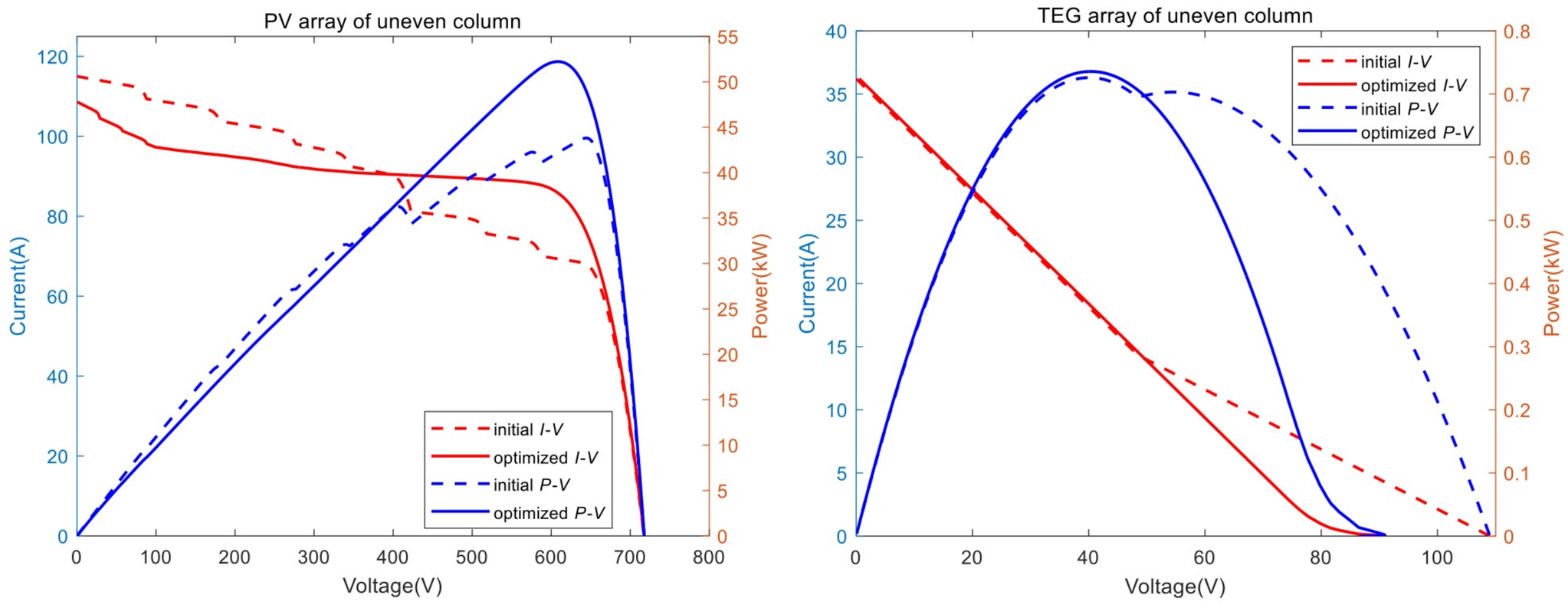

(b) Output curve under uneven column

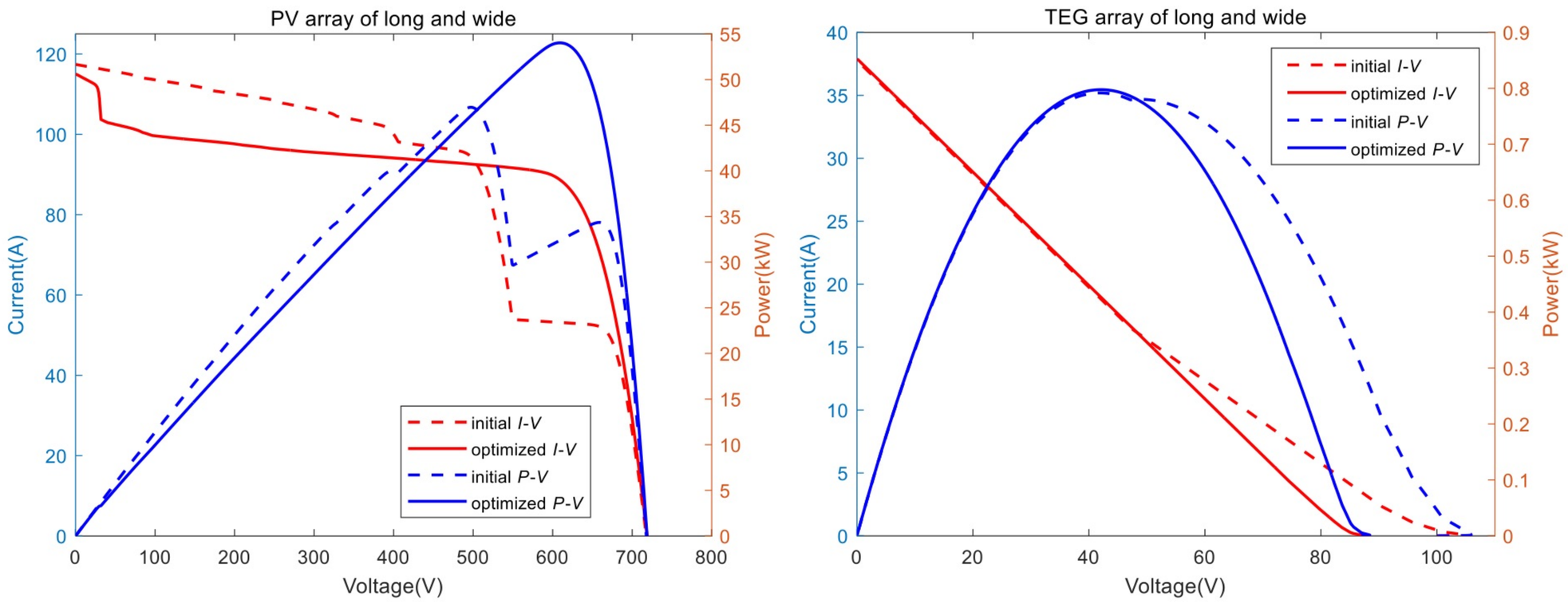

(c) Output curve under long and wide

Fig. 13. Output curve of the 20 × 15 PV-TEG array before and after reconfiguration under building shading. (a) Output curve under uneven row, (b) Output curve under uneven column, (c) Output curve under long and wide, (d) Output curve under outer, (e) Output curve under centre, (f) Output curve under random.

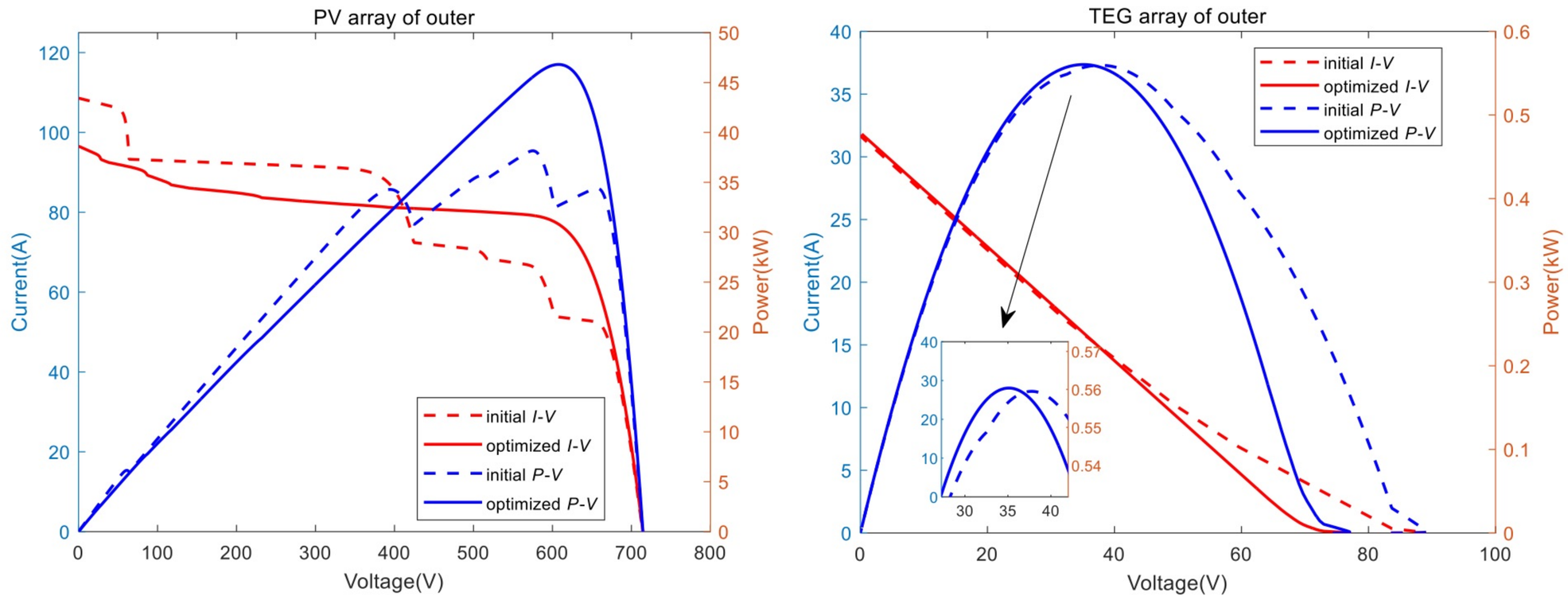

(d) Output curve under outer

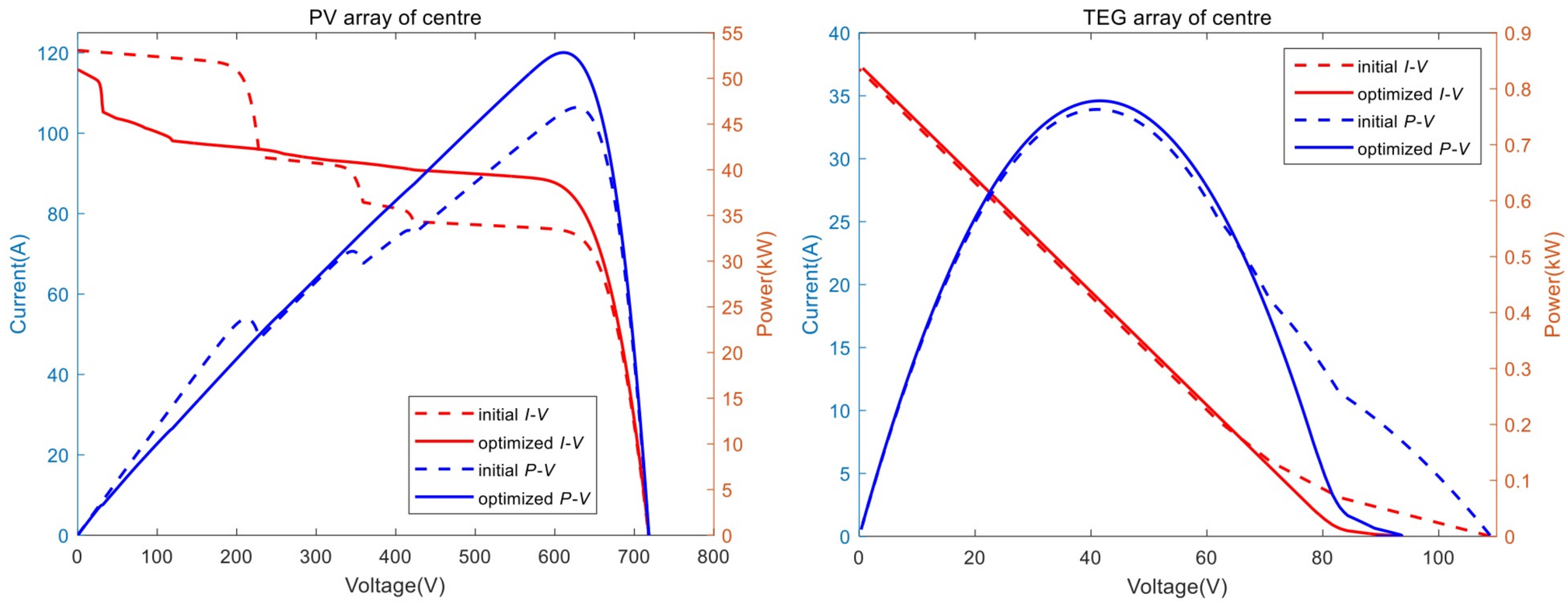

(e) Output curve under centre

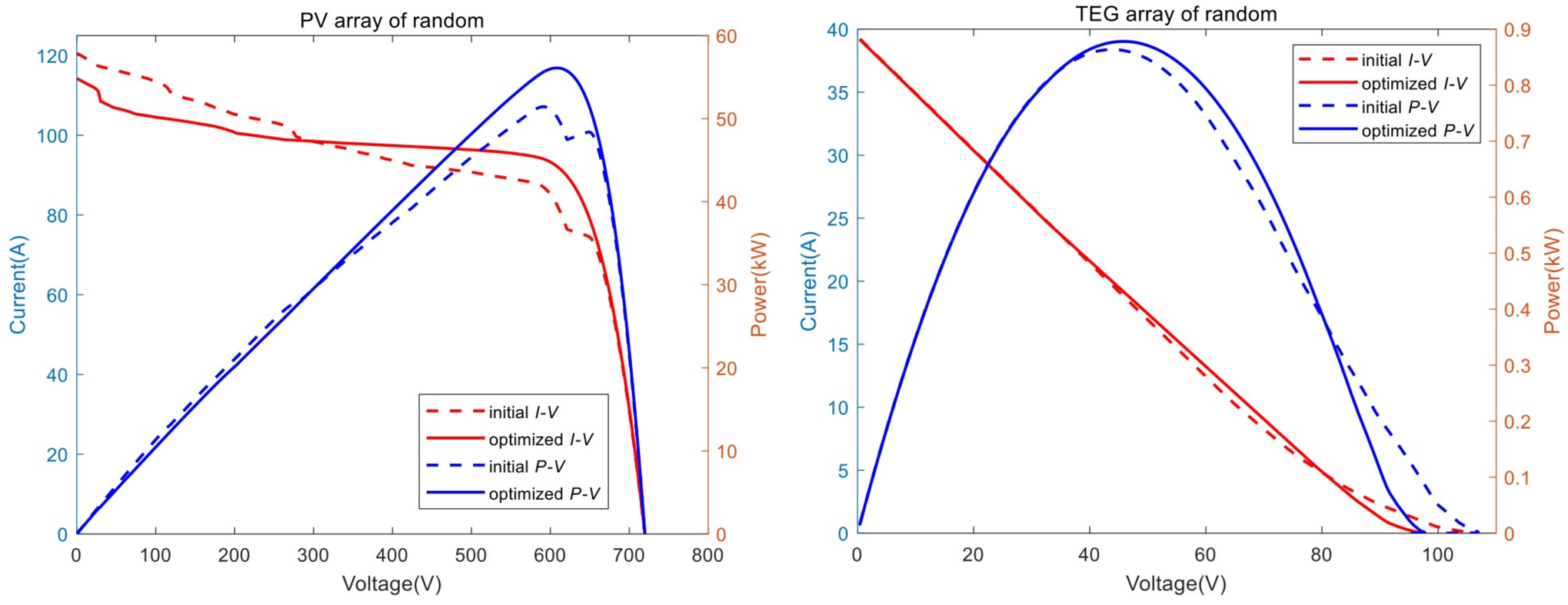

Fig. 13. (*continued*).

comparison. Meanwhile, the maximum iteration number $k_{\max\_iter}$ is set as 500 while population size N_{pop} equals to 50 for all algorithms. The ambient temperature is set at 25 °C and the ambient wind speed is set at 1.5 m/s. The details of other model parameters are shown in Table 4.

4.2. 4 × 4 symmetric small-scale system

Firstly, simulations are carried out on a hybrid PV-TEG system with 4 × 4 array size based on the shadow patterns presented in reference [42]. In detail, the tests are conducted outdoors under sunny weather

Table 6
Simulation results obtained by various algorithms.

Shadow pattern		Uneven row	Uneven column	Long and wide	Outer	Centre	Random
Before reconfiguration(kW)		38.01	40.01	44.92	35.16	44.62	48.96
ARO	P_{max}(kW)	50.45	51.34	52.76	46.18	51.86	55.09
	P_{avg}(kW)	48.89	50.76	51.65	44.97	51.52	54.28
WOA	P_{max}(kW)	49.55	51.34	52.31	44.84	51.82	54.64
	P_{avg}(kW)	48.79	50.58	51.50	44.10	50.27	54.13
PSO	P_{max}(kW)	48.65	49.54	50.60	45.29	51.37	53.74
	P_{avg}(kW)	47.42	48.67	49.25	44.08	50.31	52.95
GA	P_{max}(kW)	49.55	51.34	52.76	45.28	51.82	54.64
	P_{avg}(kW)	48.69	50.53	51.23	44.62	51.12	54.10
AOA	P_{max}(kW)	48.65	49.99	50.51	44.38	50.47	53.29
	P_{avg}(kW)	46.82	48.77	49.00	43.25	49.58	52.52
ACO	P_{max}(kW)	49.55	51.34	52.76	45.29	51.82	54.64
	P_{avg}(kW)	48.79	50.65	51.50	44.92	51.61	54.27

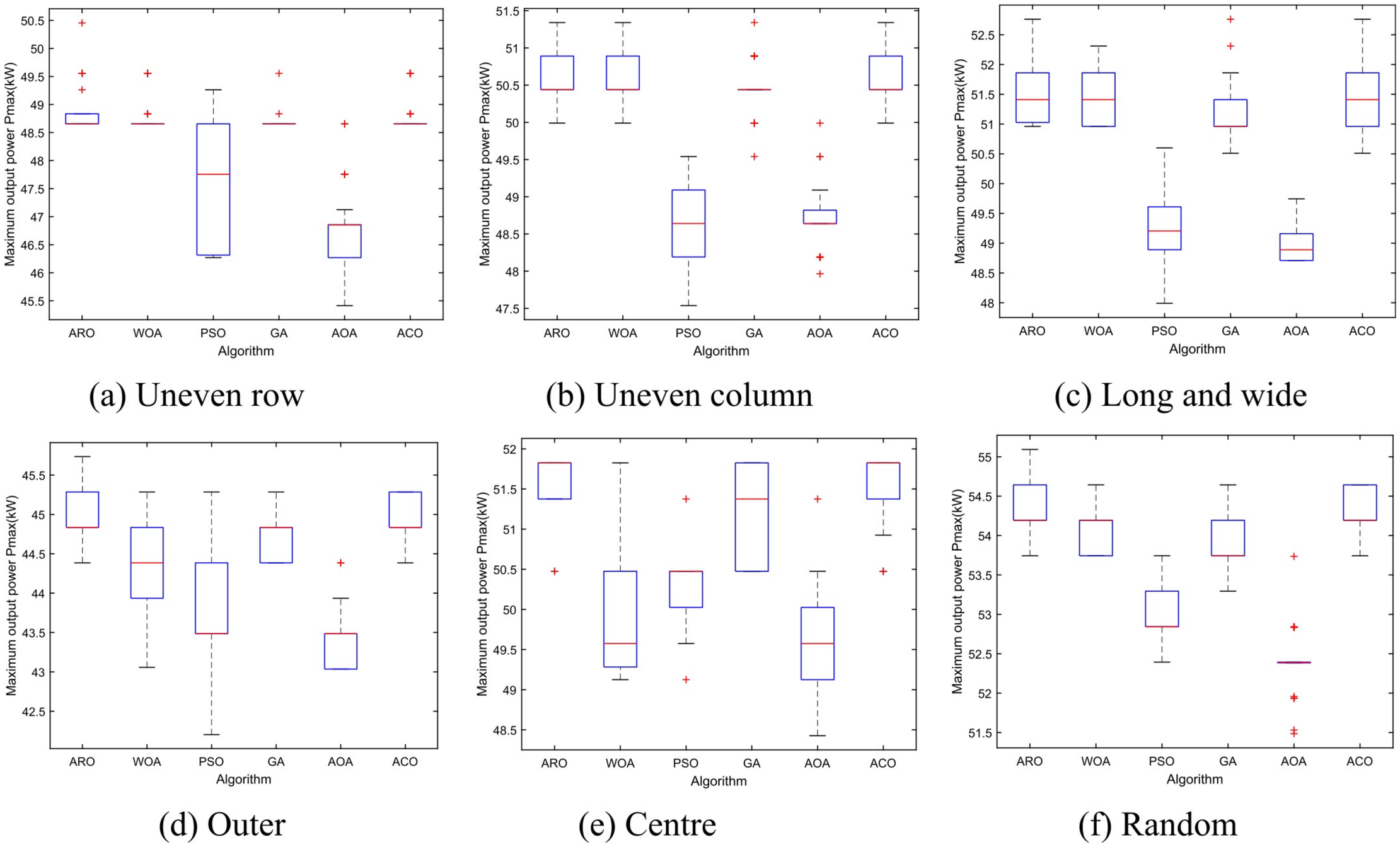

Fig. 14. Boxplots of maximum output power obtained by six algorithms under six different PSC of 20 × 15 PV-TEG hybrid system: (a) Uneven row, (b) Uneven column, (c) Long and wide, (d) Outer, (e) Centre, (f) Random.

conditions, where sixteen SL130CE-18P PV modules are selected to form a 4 × 4 PV array, as shown in Fig. 7. To simulate different PSC conditions, some of the constructed PV arrays are blocked in various degrees and modes. Meanwhile, a MESTEK/LM610 illuminometer is used to measure and record the real-time irradiance and temperature of PV arrays, and the temperature of the PV cell is estimated according to the ambient temperature and solar irradiance. Based on this, tree shading and building shading are simulated and considered in this case, for both of which the shading types include no shading, 25% shading, 50% shading, and 100% shading. ARO algorithm is applied to reconfigure PV-TEG arrays to effectively disperse the shielded area, as shown in Fig. 8. The output characteristic curve under the tree shading is shown in Fig. 9 and Fig. 10, which indicates that the multi-peak problem for both current-voltage (*I-V*) and *P-V* curves of PV array are effectively eliminated after optimization, and the maximum power point of both PV and TEG arrays are improved.

To quantitatively analyze the reconfiguration performance of the hybrid system before and after reconfiguration, Table 5 presents the output power of the hybrid PV-TEG system before reconfiguration, maximum output power (P_{max}), average output power (P_{avg}), and standard deviation (STD) after reconfiguration. It can be seen from Table 5 that after optimization under the shade of trees, the P_{max} of the hybrid system is increased from 2.31 kW to 2.76 kW, the mismatch loss is reduced from 1.4 kW to 0.95 kW, and the power of the hybrid system is increased by 19.5%. Under case of the building shading, the P_{max} of the hybrid PV-TEG system after reconfiguration is increased from 1.38 kW to 2.05 kW, the mismatch loss is reduced from 2.31 kW to 1.66 kW, and the power of the hybrid system is increased by 48.6%. Therefore, according to the simulation results, the reconfiguration method proposed in this work can indeed dramatically improve the maximum power generation.

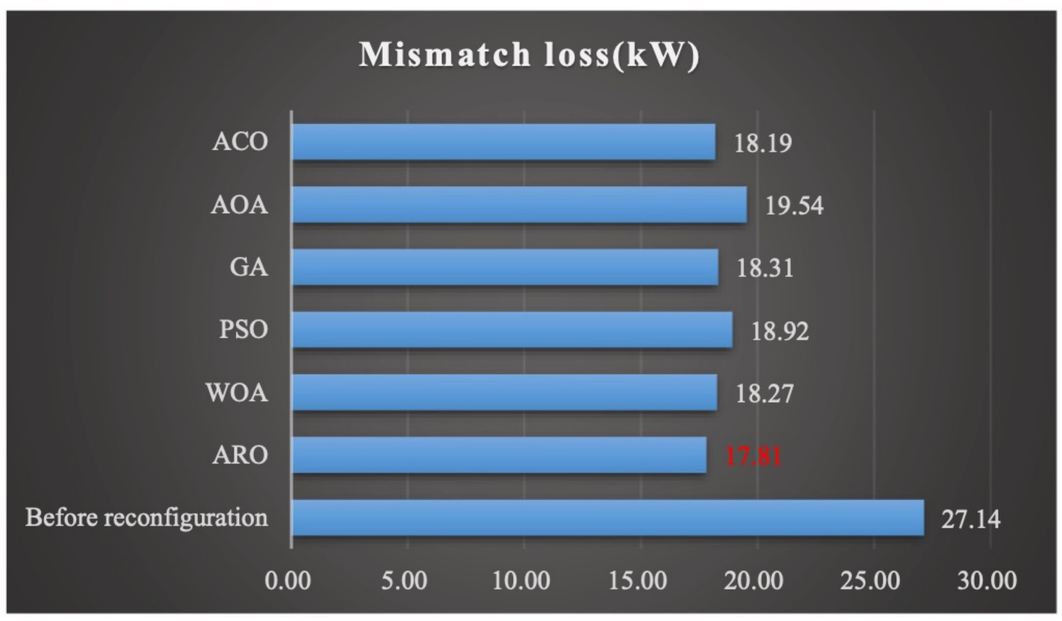

(a) Average mismatch loss

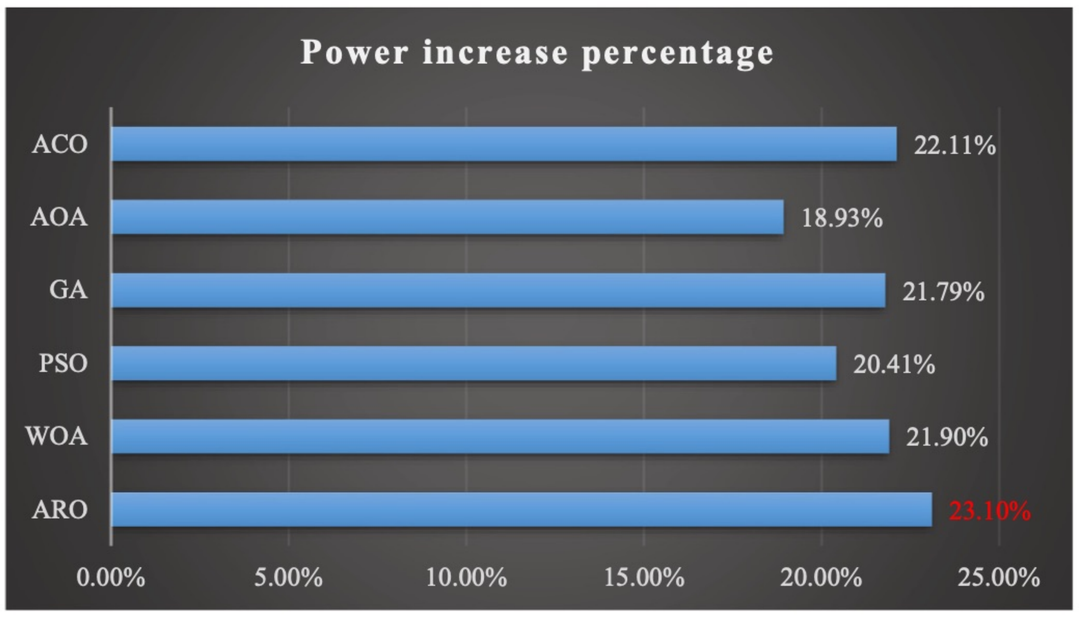

(b) Average power increase percentage

Fig. 15. Simulation results after reconfiguration of the 20 × 15 hybrid PV-TEG system.

4.3. 20 × 15 unsymmetric large-scale system

To further verify the reliability of the proposed method on a more complex and larger-scale problem, in this section, the 20 × 15 unsymmetric hybrid system is carried out for reconfiguration. The section employs six different types of PSC, as shown in Fig. 11. Fig. 12 shows the irradiation distribution after reconfiguration under different shading patterns. Fig. 12 shows that the irradiation distribution after PV and TEG array reconfiguration is more dispersed, which can effectively avoid the hotspot effect in practical engineering. The output characteristics of the 20 × 15 unsymmetric hybrid PV-TEG system before and after reconfiguration under six PSC patterns are shown in Fig. 13. Fig. 13 demonstrates that the multi-peak phenomena of *I-V* and *P-V* curves of PV arrays under different PSCs after reconfiguration are effectively suppressed. Meanwhile, P_{max} of the PV and TEG array are both enhanced after reconfiguration. Therefore, the proposed ARO algorithm based reconfiguration method can effectively alleviate the adverse impacts of PSC on the unsymmetric hybrid PV-TEG system, and thus improve the system performance.

In addition, five other well-known algorithms including GA, PSO, AOA, ACO, and WOA are employed for performance comparison with ARO based on the same hybrid system. Simulation results are detailed in Table 6, in which the P_{max} and P_{avg} are selected as evaluation indicators, which shows that ARO algorithm under all the six types of PSC performs better than its competitors for basically all indicators. The boxplots of maximum output power obtained by six algorithms under six different PSC of a 20 × 15 PV-TEG hybrid system are shown in Fig. 14. As shown in Fig. 14, ARO can obtain the highest output power and average output power over the 30 independent runs compared with other algorithms. It is noteworthy that the results obtained by ACO are similar to ARO under most PSC patterns, but the overall execution speed of ACO lags far behind that of ARO. In detail, ACO takes about 500 s for 30 independent runs, while ARO merely takes about 200 s. Fig. 15 shows the average mismatch loss and average power growth percentage of the five algorithms after reconfiguration in a 20 × 15 hybrid system. As shown in Fig. 15(a), the average mismatch loss acquired by ARO, WOA, PSO, GA, AOA, and ACO algorithms are 17.81, 18.27, 18.92, 18.31, 19.54, and 18.19, respectively. In addition, as can be seen from Fig. 15(b), after a reconfiguration by ARO, WOA, PSO, GA, AOA, and ACO, the average power increase percentage of the hybrid PV-TEG system reach 23.10%, 21.90%, 20.41%, 21.79%, 18.93%, and 22.11%, respectively. Therefore, according to the detailed simulation results, it can be concluded that ARO based reconfiguration method can achieve the most satisfactory dynamic reconfiguration scheme of the 20 × 15 unsymmetric hybrid PV-TEG system under different shadow patterns.

4.4. Discussion

The reconfiguration of the PV-TEG hybrid system is a complicated and highly nonlinear optimization problem, thus traditional mathematical methods are inadequate to solve this problem due to their poor global optimum searching ability and large computation burden. In contrast, the intelligent optimization algorithm adopted in this study has the merits of high convergence speed and strong global searching ability. Fig. 9, Fig. 10, and Table 5 quantitatively demonstrate that the reconfiguration scheme based on the intelligent optimization can reduce

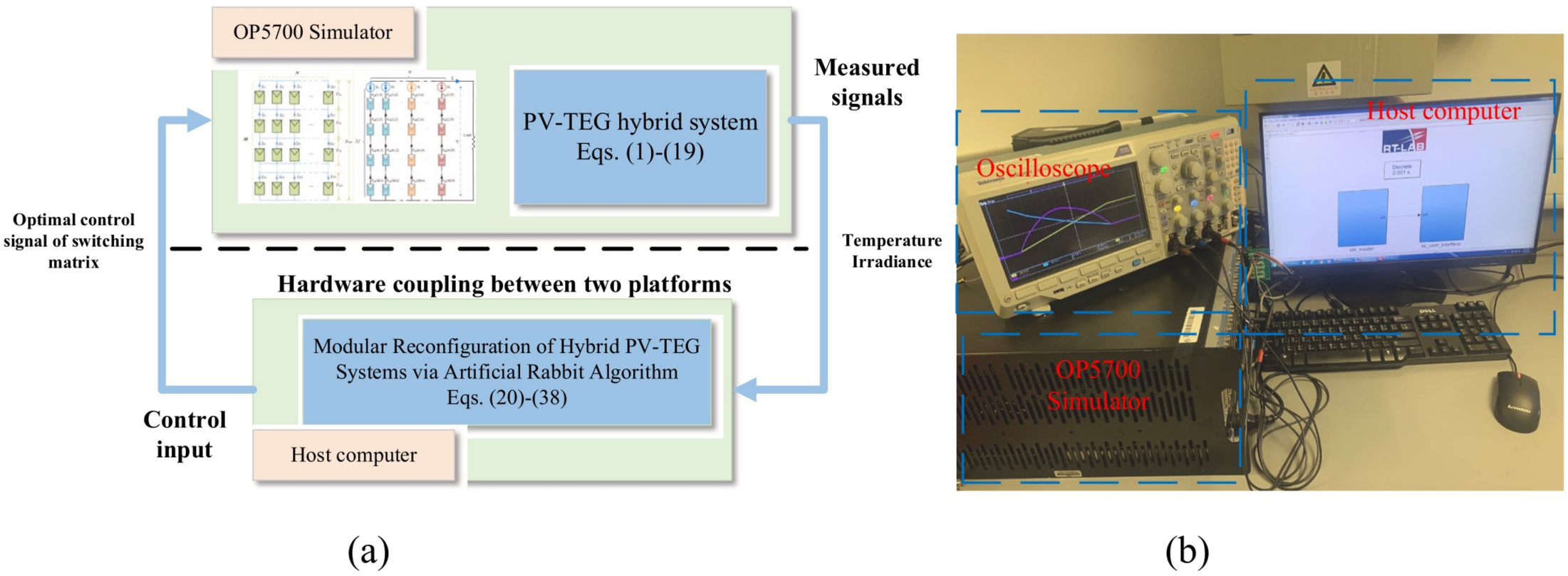

Fig. 16. HIL experiment based on RTLAB platform: (a) HIL experiment diagram, (b) hardware platform of the HIL experiment.

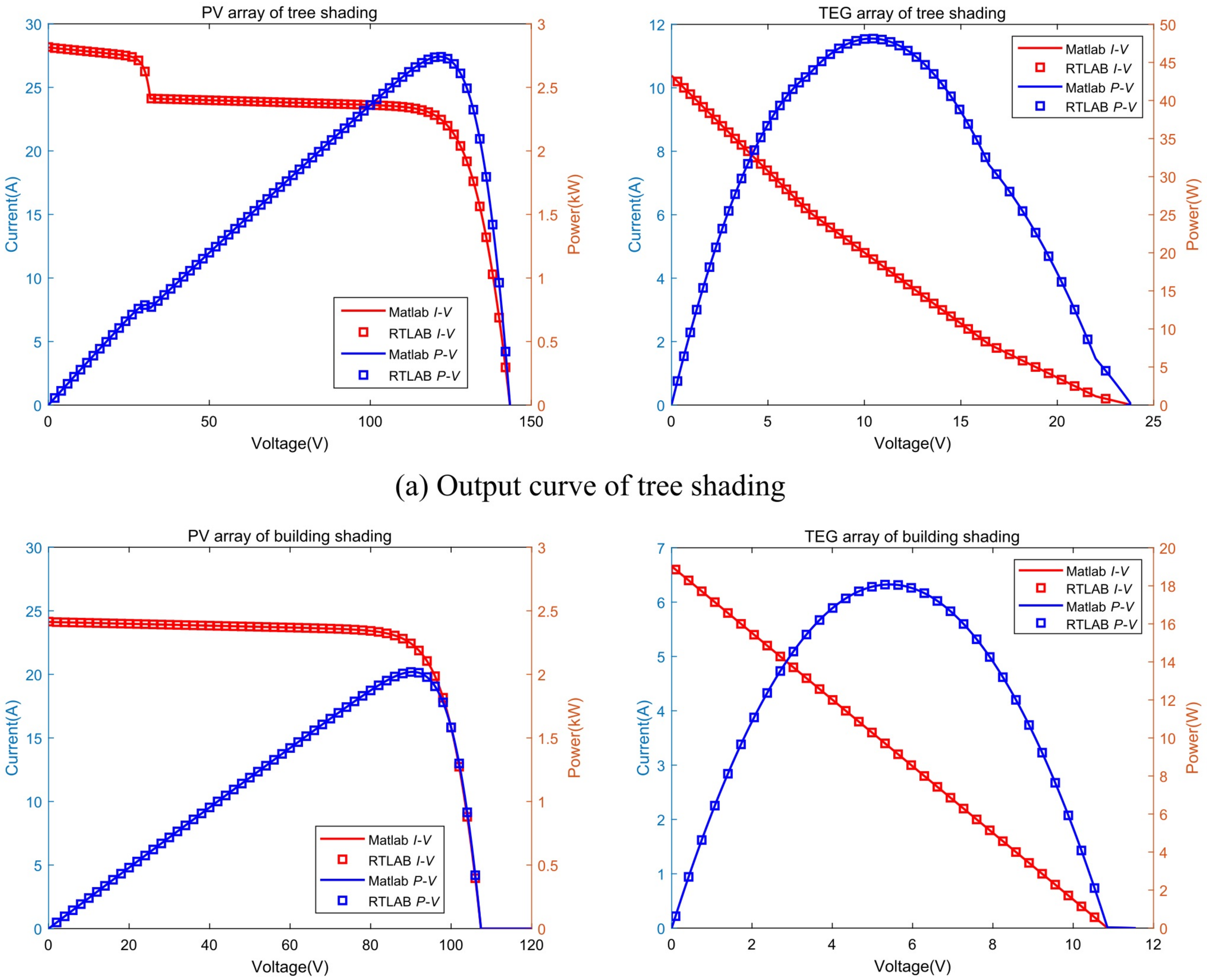

(a) Output curve of tree shading

(b) Output curve of building shading

Fig. 17. Simulation results and HIL test results of 4 × 4 PV-TEG system. (a) Output curve of tree shading and (b) Output curve of building shading.

the adverse effects of PSC, and then effectively improve the output power of the PV-TEG hybrid system. In Section 4.3, six intelligent algorithms including ARO, PSO, GA, AOA, WOA, and ACO are used to solve the reconfiguration problem under six different PSC patterns, respectively. It can be seen from Fig. 15 and Table 6 that ARO algorithm obtains the optimal reconfiguration scheme under all six PSC patterns. The main reason is that compared with other intelligent optimization algorithms, an energy factor mechanism is employed in ARO algorithm during iterations that can help more effectively balance the global exploration and local exploitation. As a result, according to the boxplots in Fig. 14, it is obvious that ARO algorithm also shows higher convergence stability compared with other competitors. Although the results obtained by ACO algorithm are similar to ARO under most PSC patterns, but the overall execution speed of the ACO algorithm lags far behind that of ARO. In detail, ACO takes about 600 s for 30 independent runs, while ARO merely takes about 200 s. However, ARO as a typical metaheuristic algorithm, also has some inevitable limitations for its optimization, such as strict parameters settings including the initial population scale and iteration criterion design. In addition, there is a degree of randomness in the convergence of the algorithm that may lead to different optimal results for some iterations.

5. HIL test

To validate the hardware feasibility of the proposed method, HIL experiments are carried out on RTLAB platform in this study. The testing environment of the RTLAB experiment platform is shown in Fig. 16, and the sampling frequency is set as 1 kHz. Meanwhile, the data obtained from Matlab/Simulink platform is used as the comparison data to observe the running results acquired from RTLAB platform. Fig. 17 and Fig. 18 show the output characteristic curves of 4 × 4 and 20 × 20 mixed PV-TEG system after reconfiguration, respectively. According to comparison of the output characteristic curves obtained by Matlab/Simulink and RTLAB platforms in Fig. 17 and Fig. 18, it is obvious that their curves under various PSC patterns are all highly consistent, which means they have very similar responses and performance Therefore, this high degree of fitting can proved that the proposed method owns desirable hardware feasibility under various PSC patterns, which owns promising practical engineering implementation value and feasibility.

6. Conclusion

This paper proposes a modular reconfiguration method for the hybrid system based on ARO algorithm to alleviate the negative effects caused by partial shielding condition (PSC), which is verified that can

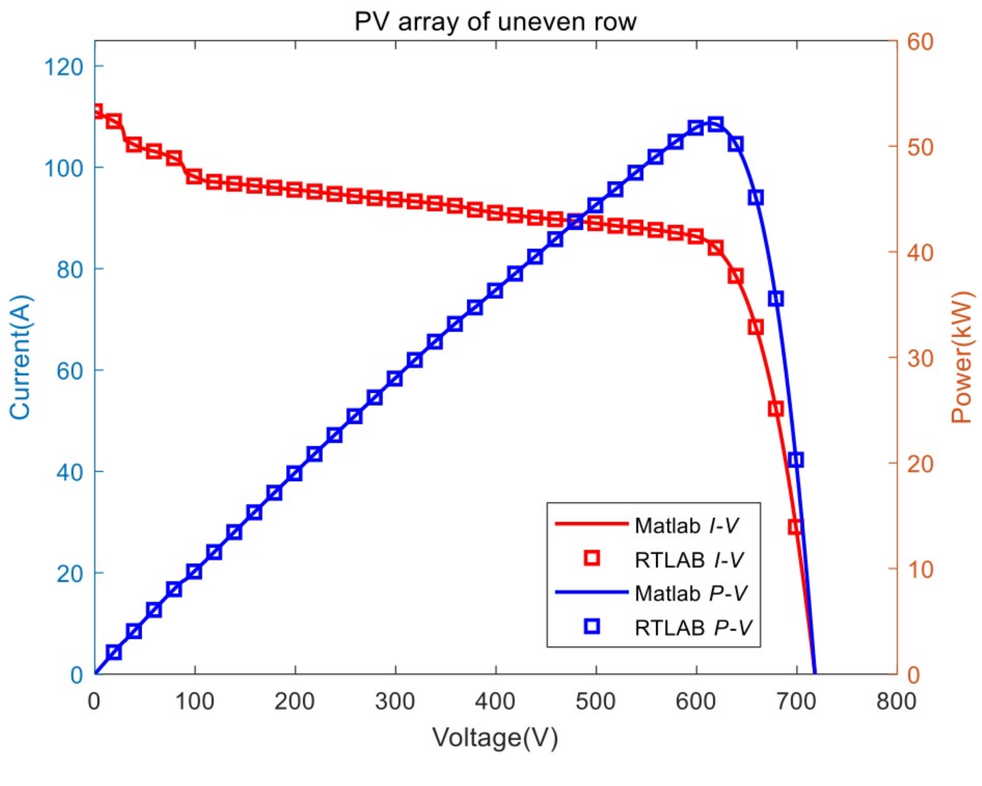

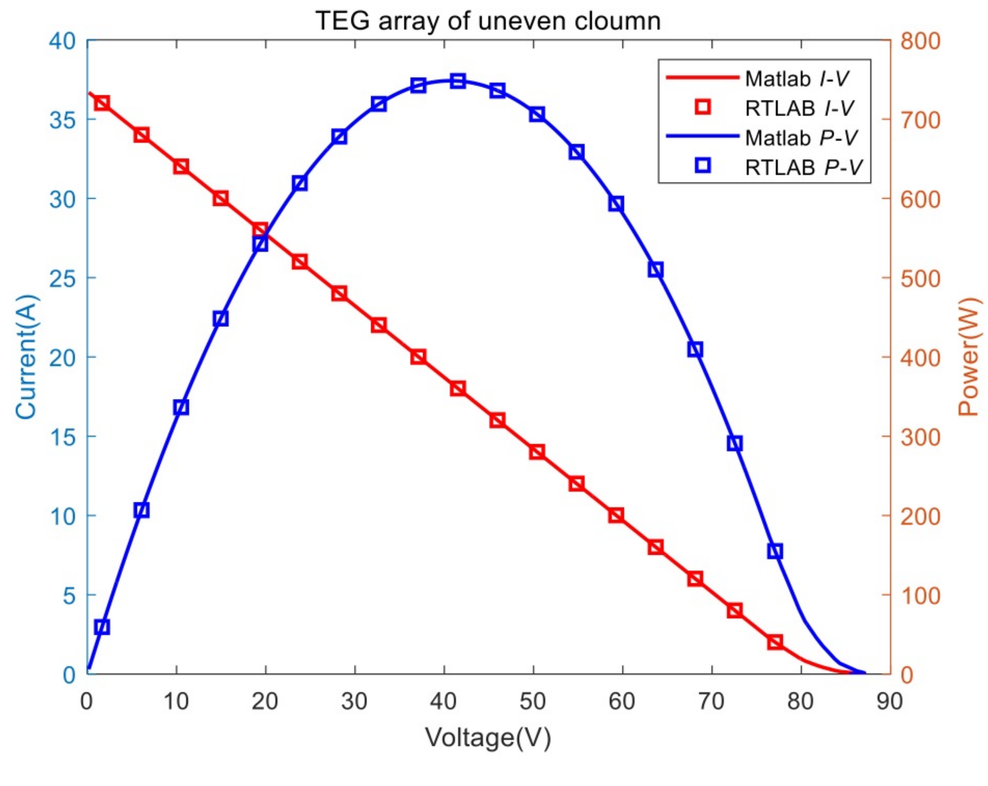

(a) Output curve of uneven row

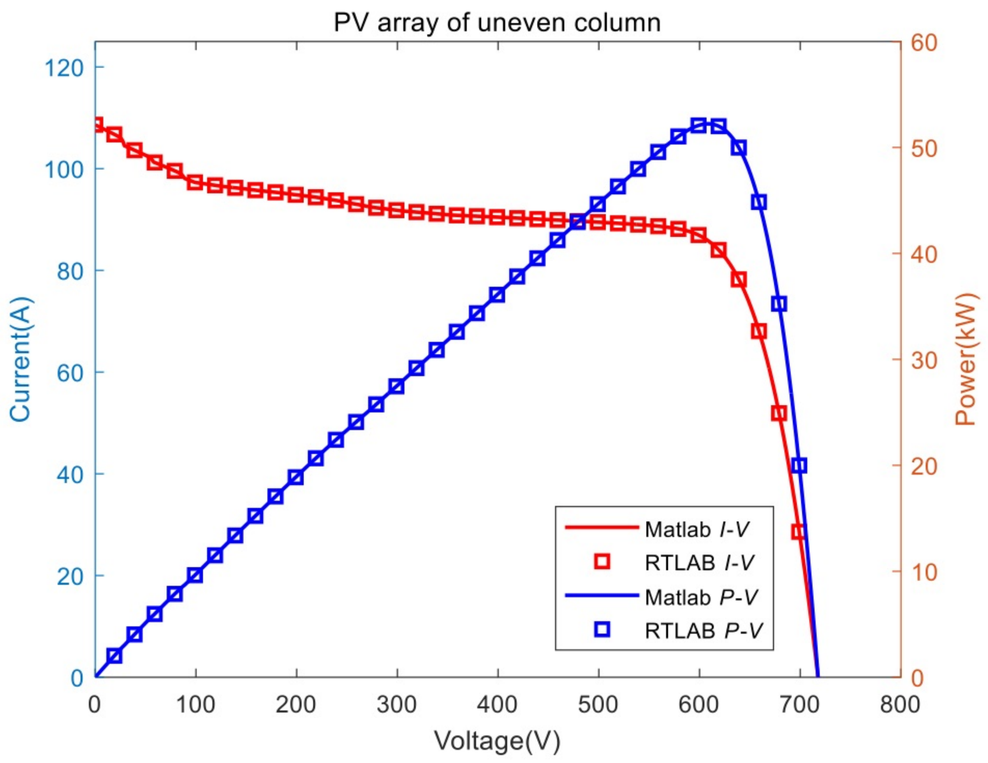

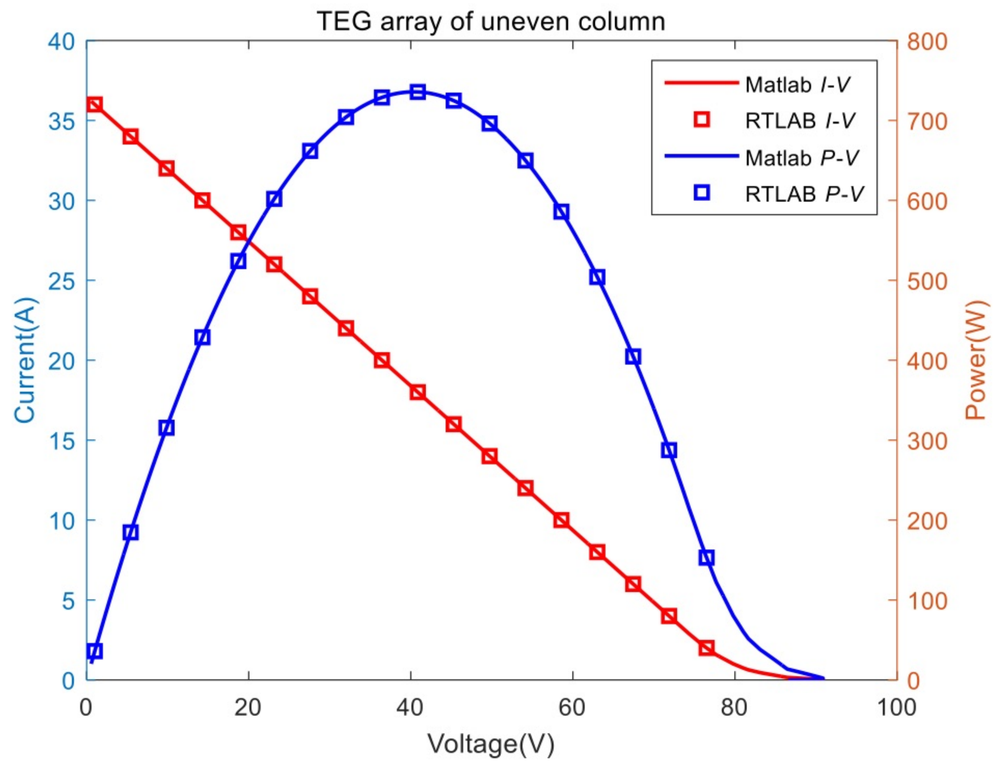

(b) Output curve of uneven column

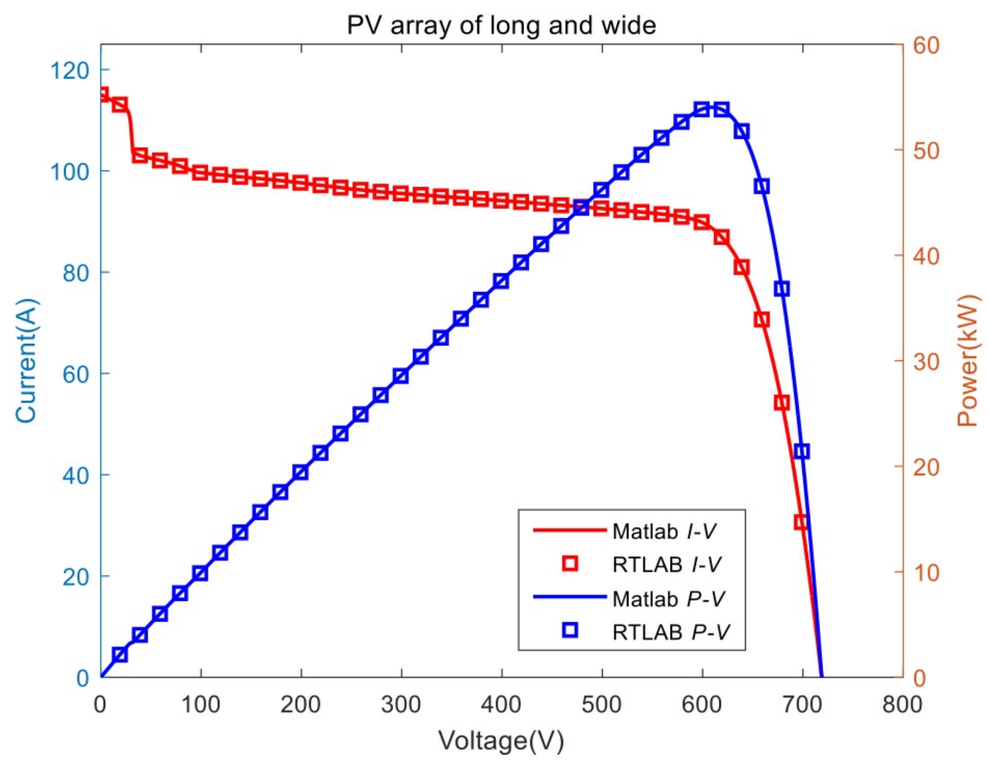

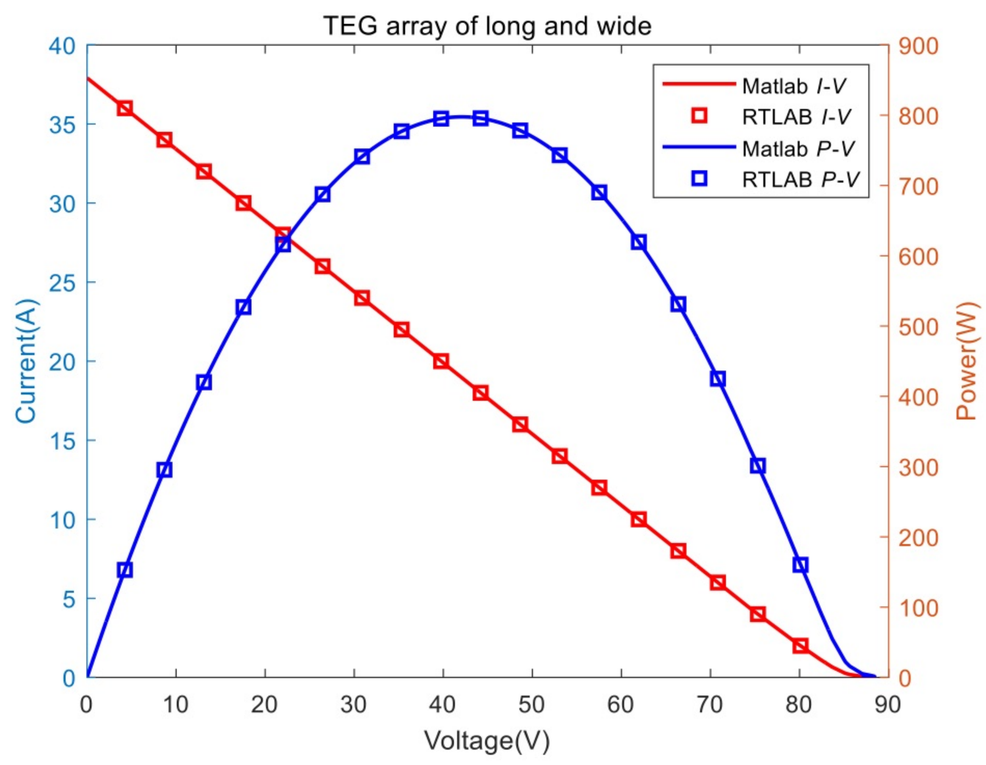

(c) Output curve of long and wide

Fig. 18. Simulation results and HIL test results of the 20 × 15 hybrid system. (a) Output curve of uneven row, (b) Output curve of uneven column, (c) Output curve of long and wide, (d) Output curve of outer, (e) Output curve of outer, (f) Output curve of random.

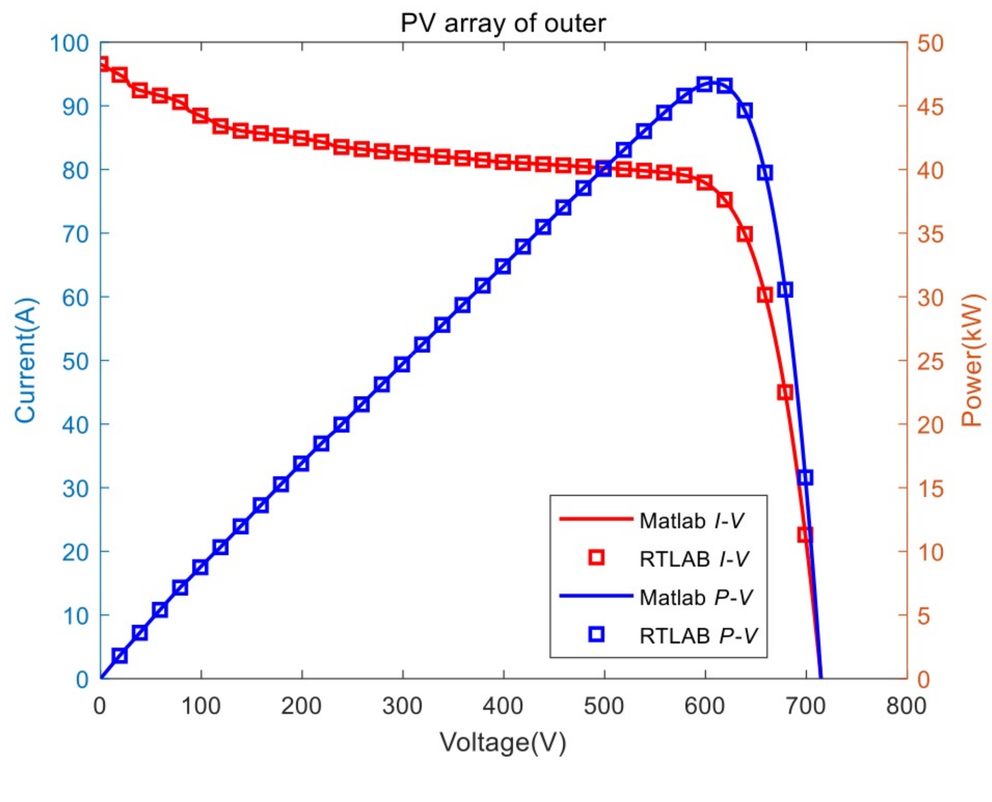

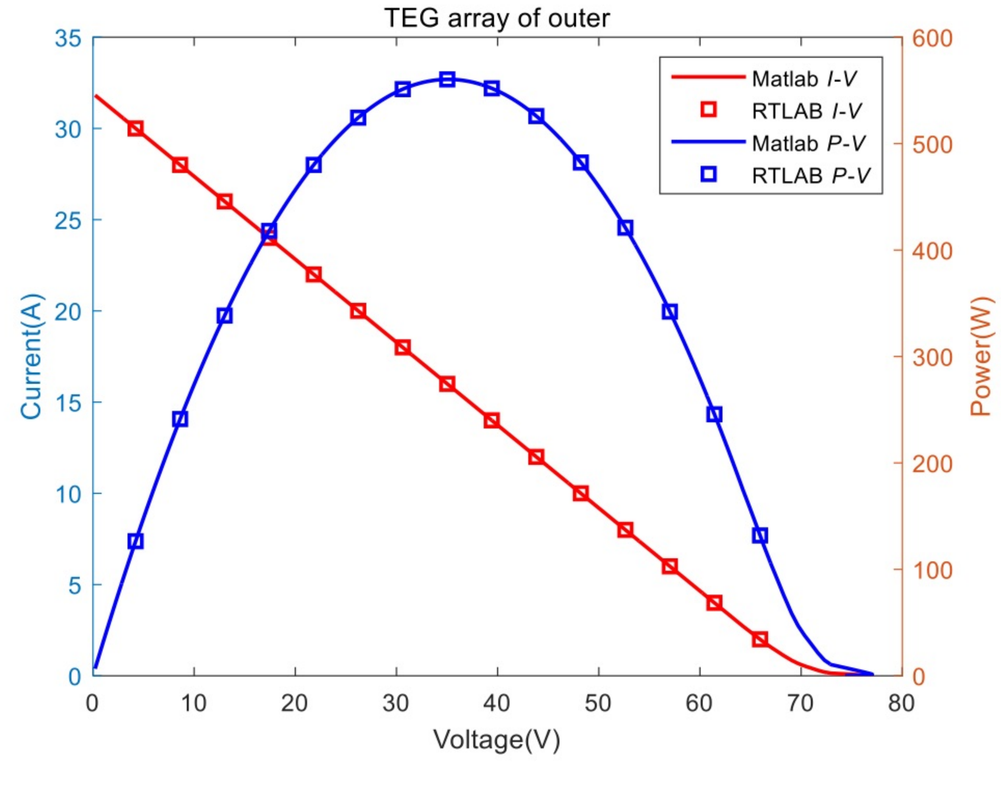

(d) Output curve of outer

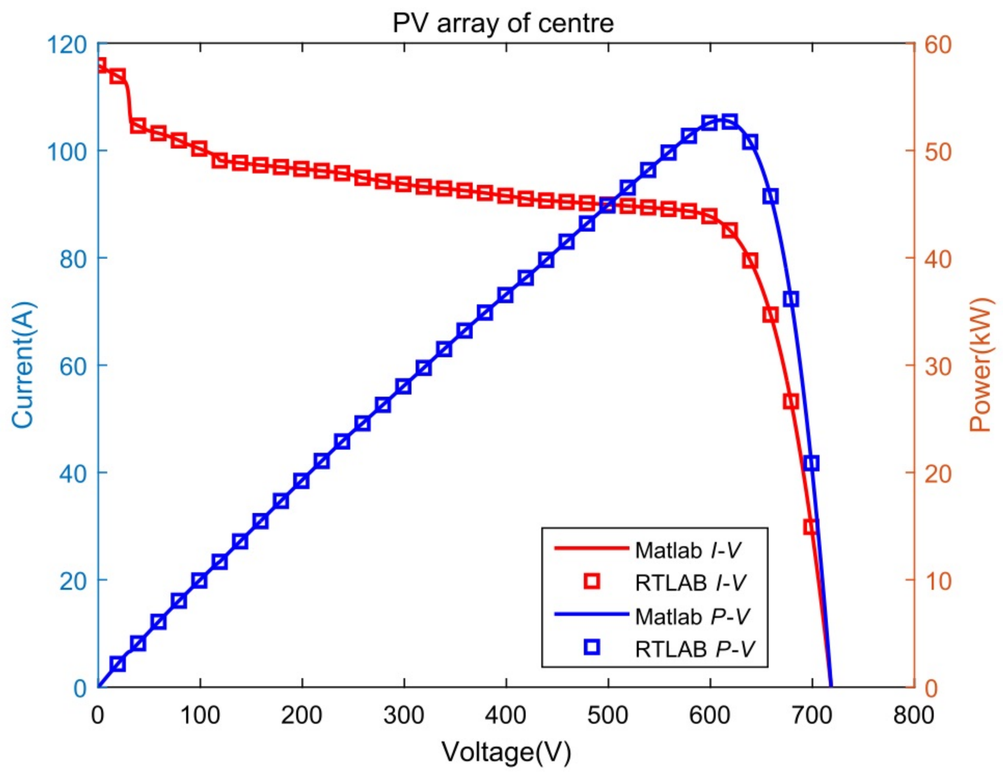

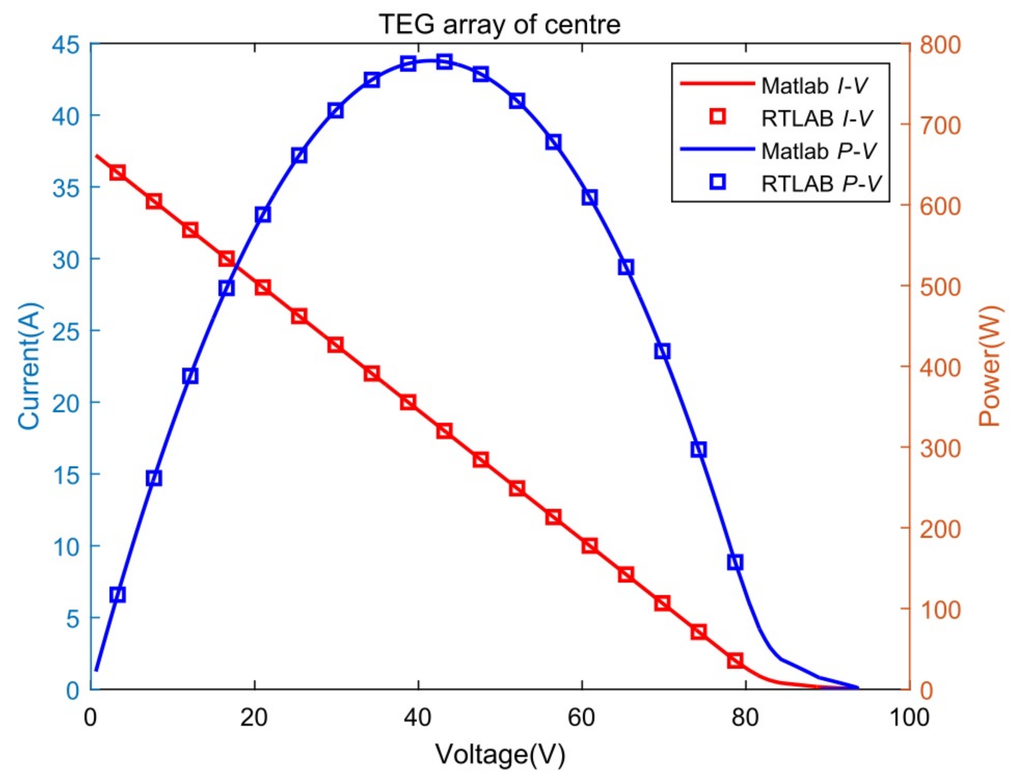

(e) Output curve of outer

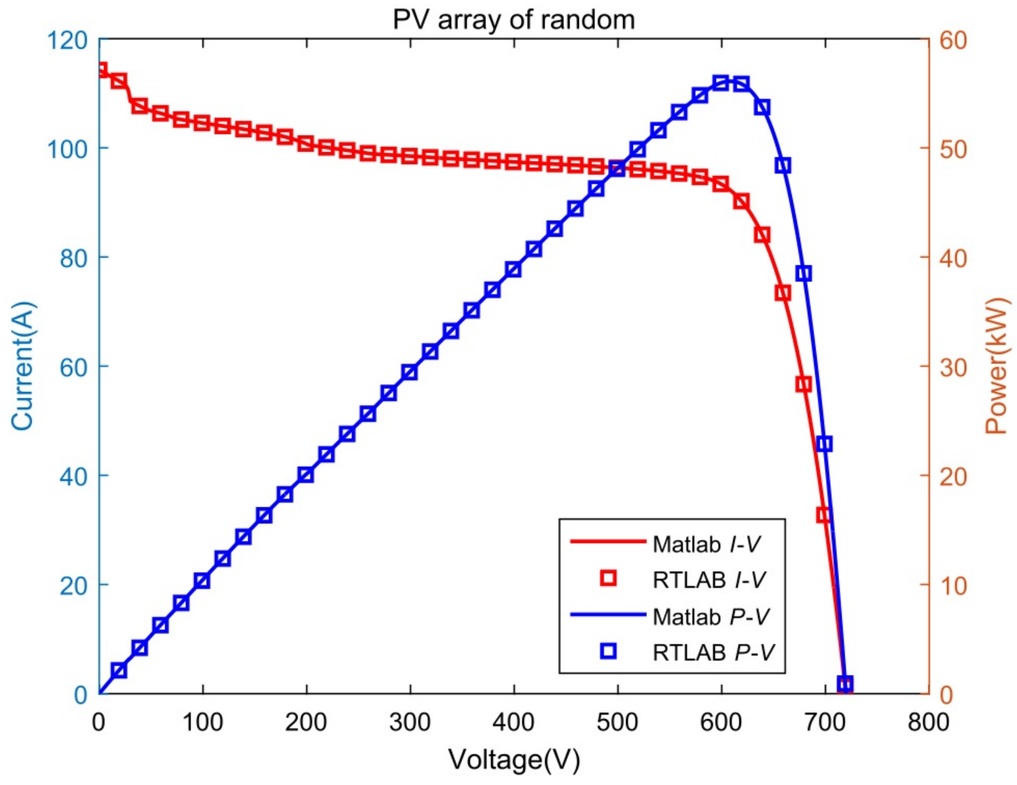

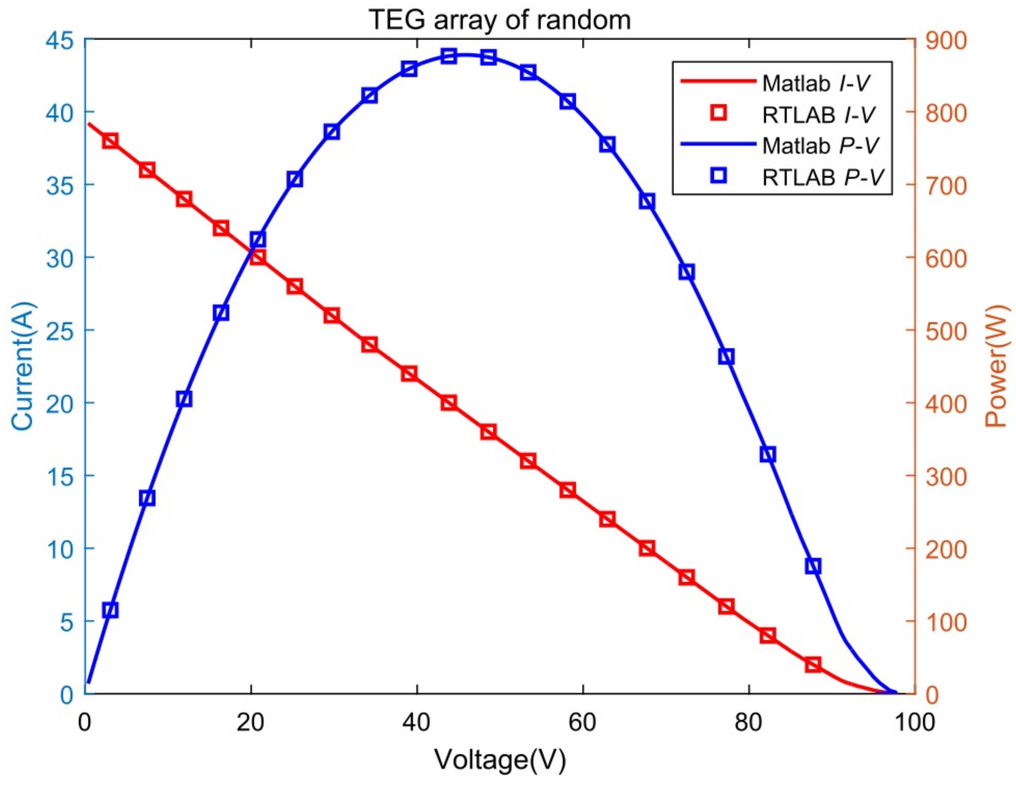

(f) Output curve of random

Fig. 18. (*continued*).

effectively improve the output performance of the hybrid system. The main contributions of this work are as follows:

I. A hybrid PV-TEG system model is introduced and constructed in this work, which aims to properly utilize the excess heat dissipated from the PV panel during the power generation of the PV system to enhance energy conversion efficiency while ensuring its healthy operation;
II. A modular reconfiguration scheme for hybrid PV-TEG systems is proposed, in which the PV and TEG array components are modularized to reduce the number of switches required for reconfiguration, thus reducing the overall costs;
III. This work devises a reconfiguration method for hybrid systems based on ARO algorithm. Compared with the power output obtained before reconfiguration, the maximum power of 4 × 4 and 20 × 15 hybrid PV-TEG systems after reconfiguration by ARO algorithm is increased by 34.05% and 23.10%, respectively. Meanwhile, according to the mismatch loss and power increase percentage, the reconfiguration performance of ARO algorithm shows superior performance than other well-known algorithms such as GA, PSO, AOA, ACO and WOA;
IV. The HIL experiment based on RTLAB platform is undertaken to further prove the implementation feasibility of the proposed reconfiguration strategy.

Future research will focus on the following three aspects:

I. In the future, a small-scale PV-TEG hybrid system real test bench will be constructed to further verify the full hardware application feasibility of the proposed hybrid system and reconfiguration method;
II. The reconfiguration method proposed in this paper can also be applied to other research objects for power generation performance optimization in the future, including batteries, electrolytic cells and so on;
III. At present, the PV-TEG hybrid system mainly includes stacking and spectrum splitting. In future studies, the application of spectral splitting method based reconfiguration strategy for the PV-TE hybrid system will be considered, which is expected to further decrease the adverse effect of temperature rise on the PV system and more sufficiently utilize waste heat for power generation.

CRediT authorship contribution statement

Bo Yang: Writing – review & editing, Writing – original draft, Conceptualization. **Yulin Li:** Writing – original draft, Data curation. **Jianxiang Huang:** Funding acquisition, Formal analysis. **Miwei Li:** Visualization, Data curation. **Ruyi Zheng:** Visualization, Data curation. **Jinhang Duan:** Methodology, Data curation. **Tingsheng Fan:** Investigation, Resources. **He Zou:** Resources, Validation. **Tao Liu:** Resources. **Jingbo Wang:** Writing – review & editing, Supervision. **Hongchun Shu:** Supervision, Resources. **Lin Jiang:** Supervision.

Declaration of Competing Interest

The authors declare that they have no known competing financial interests or personal relationships that could have appeared to influence the work reported in this paper.

Data availability

No data was used for the research described in the article.

Acknowledgments

This work is supported by National Natural Science Foundation of China (61963020, 62263014) and Yunnan Provincial Basic Research Project (202201AT070857).

References

[1] Yang B, Zhu TJ, Wang JB, et al. Comprehensive overview of maximum power point tracking algorithms of PV systems under partial shading condition. J Clean Prod 2020;268:121983.
[2] Singh S, Saini S, Gupta SK, Kumar B. Solar-PV inverter for the overall stability of power systems with intelligent MPPT control of DC-link capacitor voltage. Protect Control Modern Power Syst 2023;8:15.
[3] Yang B, Li YL, Li JL, et al. Comprehensive summary of solid oxide fuel cell control: a state-of-the-art review. Protect Control Modern Power Syst 2022;7(36):1–31.
[4] Yin XX, Lei MZ. Jointly improving energy efficiency and smoothing power oscillations of integrated offshore wind and photovoltaic power: a deep reinforcement learning approach. Protect Control Modern Power Syst 2023;8(2):420–30.
[5] Yang B, Liu BQ, Zhou HY. A critical survey of technologies of large offshore wind farm integration: summarization, advances, and perspectives. Protect Control Modern Power Syst 2022;7(17):1–32.
[6] Zhang YX, Zhu N, Zhao XD, et al. Energy performance and enviroeconomic analysis of a novel PV-MCHP-TEG system. Energy 2022;274:127342.
[7] Gopinath M, Marimuthu R. PV-TEG output: comparison with heat sink and graphite sheet as heat dissipators. Case Stud Thermal Eng 2023;45:102935.
[8] Cai Y, Wang L, Wang WW, et al. Solar energy harvesting potential of a photovoltaic-thermoelectric cooling and power generation system: bidirectional modeling and performance optimization. J Clean Prod 2020;254:120150.
[9] Yang B, Zeng CY, Li DY, et al. Improved immune genetic algorithm based TEG system reconfiguration under non-uniform temperature distribution. Appl Energy 2022;325:119691.
[10] Chandel R, Chandel SS, Prasad D, et al. Review on thermoelectric systems for enhancing photovoltaic power generation. Sustain Energy Technol Assess 2022;53:102585.
[11] Liao TJ, Lin BH, Yang ZM. Performance characteristics of a low concentrated photovoltaic-thermoelectric hybrid power generation device. Int J Thermal Sci 2014;77:158–64.
[12] Attivissimo F, Nisio AD, Lanzolla AML, et al. Feasibility of a photovoltaic–thermoelectric generator: performance analysis and simulation results. IEEE Trans Instrument Measure 2015;64(5):1158–69.
[13] Zhang XN, Huang YW, Chen Z. A hybrid system integrating photovoltaic module and thermoelectric devices for power and cooling cogeneration. Solar Energy 2022;239:350–8.
[14] Yin E, Li Q. Multi-objective optimization of a concentrated spectrum splitting photovoltaic-thermoelectric hybrid system. Appl Therm Eng 2023;219:119518.
[15] Bollipo RB, Mikkili S, Bonthagorla PK. Hybrid, optimal, intelligent and classical PV MPPT techniques: a review. CSEE J Power Energy Syst 2021;7(1):9–33.
[16] Yang B, Ye HY, Wang JB, et al. PV arrays reconfiguration for partial shading mitigation: recent advances, challenges and perspectives. Energ Conver Manage 2021;247:114738.
[17] Manna S, Akella AK, Singh DK. Novel Lyapunov-based rapid and ripple-free MPPT using a robust model reference adaptive controller for solar PV system. Protect Control Modern Power Syst 2023;8(13):1–25.
[18] Gong L, Hou G, Huang C. A two-stage MPPT controller for PV system based on the improved artificial bee colony and simultaneous heat transfer search algorithm. ISA Trans 2023;132:428–43.
[19] Lashab A, Sera D, Guerrero JM. A dual-discrete model predictive control-based MPPT for PV systems. IEEE Trans Power Electron 2019;34(10):9686–97.
[20] Yang B, Shao R, Zhang M, et al. Socio-inspired democratic political algorithm for optimal PV array reconfiguration to mitigate partial shading. Sustain Energy Technol Assess 2021;48:101627.
[21] Rezazadeh S, Moradzadeh A, Pourhossein K, et al. Photovoltaic array reconfiguration under partial shading conditions for maximum power extraction: a state-of-the-art review and new solution method. Energ Conver Manage 2022;258:115468.
[22] Fathy A. Butterfly optimization algorithm based methodology for enhancing the shaded photovoltaic array extracted power via reconfiguration process. Energ Conver Manage 2020;220:113115.
[23] Guo TZ, Feng TB, Zhang X, et al. Dynamic reconfiguration method of TCT photovoltaic array based on peak power evaluation. Power Syst Technol 2022;46(11):4415–22.
[24] Yang B, Zhang MT, Guo ZX, et al. Adaptive evolutionary jellyfish search algorithm based optimal photovoltaic array reconfiguration under partial shading condition for maximum power extraction. Expert Syst Appl 2023;215:119325.
[25] Krishna GS, Moger T. Reconfiguration strategies for reducing partial shading effects in photovoltaic arrays: state of the art. Solar Energy 2019;182:429–52.
[26] Yang B, Wu SC, Li Q, et al. Jellyfish search algorithm based optimal thermoelectric generation arrays reconfiguration under non-uniform temperature distribution condition. Renew Energy 2023;204:197–217.
[27] Li F, Meng SF. ICL static reconstruction method of photovoltaic array under partial shadow condition. Elect Power Automat Equip 2021;41(8):82–8.

[28] Ahmed MN, Essam HH, Bahaa EH, et al. Optimal reconfiguration strategy based on modified Runge Kutta optimizer to mitigate partial shading condition in photovoltaic systems. Energy Rep 2022;8:7242–62.
[29] Chen YJ, Yang B, Guo ZX, et al. Dynamic reconfiguration for TEG systems under heterogeneous temperature distribution via adaptive coordinated seeker. Protect Control Modern Power Syst 2022;7:38.
[30] Guo ZX, Yang B, Chen YJ, et al. Modular thermoelectric generation arrays reconfiguration under heterogeneous temperature distribution via improved cooperation search algorithm: modelling, design and HIL validation. Appl Therm Eng 2023;219(A):119323.
[31] Luo D, Liu ZR, Yan YY, et al. Recent advances in modeling and simulation of thermoelectric power generation. Energ Conver Manage 2022;273:116389.
[32] Muzathik AM. Photovoltaic modules operating temperature estimation using a simple correlation. Int J Energy Eng 2014;4(4):151–8.
[33] Zhu Z, Hou MY, Ding L, et al. Optimal photovoltaic array dynamic reconfiguration strategy based on direct power evaluation. IEEE Access 2020;8:210267–76.
[34] Wang LY, Gao QJ, Zhang ZX, et al. Artificial rabbits optimization: a new bio-inspired meta-heuristic algorithm for solving engineering optimization problems. Eng Appl Artif Intel 2022;114:105082.
[35] Dangi D, Chandel ST, Dixit DK, et al. An efficient model for sentiment analysis using artifcial rabbits optimized vector functional link network. Expert Syst Appl 2023;225:119849.
[36] Liu HT, Zhai RR, Fu JX, et al. Optimization study of thermal-storage PV-CSP integrated system based on GA-PSO algorithm. Solar Energy 2019;184:391–409.
[37] Kornelakis A, Marinakis Y. Contribution for optimal sizing of grid-connected PV-systems using PSO. Renew Energy 2010;35(6):1333–41.
[38] Ajmal AM, Ramachandaramurthy VK, Naderipour A, et al. Comparative analysis of two-step GA-based PV array reconfiguration technique and other reconfiguration techniques. Energ Conver Manage 2021;230:113806.
[39] Mirjalili S, Lewis A. The whale optimization algorithm. Adv Eng Software 2016;95:51–67.
[40] Tan WH, Saleh JM. A hybrid whale optimization algorithm based on equilibrium concept. Alex Eng J 2023;68:763–86.
[41] Abualigah L, Diabat A, Mirjalili S, et al. The arithmetic optimization algorithm. Comput Methods Appl Mech Eng 2021;376:113609.
[42] Yao F, Fu Y, Li ZG. Optimal reconfiguration of total-cross-tied PV array based on multi-knapsack problem. Acta Energiae Solaris Sinica 2021;42(8):200–7.